UNIVERSIDADE DE ÉVORA

Fragmentation During Primordial Star Formation

Jayanta Dutta

Thesis submitted to the University of Évora
for obtaining PhD degree in Earth and Space Sciences
specialization in Astronomy and Astrophysics

Évora, February 2016

Institute for Advanced Studies and Research (IIFA)

UNIVERSITY OF ÉVORA
INSTITUTE FOR ADVANCED
STUDIES AND RESEARCH

DECLARATION

I hereby declare that Dr. **Jayanta Dutta** has successfully defended his PhD thesis in Earth and Space Sciences of University of Évora with the title "Fragmentation during primordial star formation", on December 19th, 2016.

Dr. Jayanta Dutta has obtained the classification of "Approved with Distinction and Praise" that correspond to the highest classification.

This declaration doesn't replace the Doctoral Certificate issued by the Academic Services of the University of Évora.

University of Évora, December 19th, 2016

The Head of the Division of the Institute of Advanced Studies and Research

UNIVERSIDADE DE ÉVORA
Instituto de Investigação
e Formação Avançada (IIFA)

Maria Cláudia Magalhães da Cruz Bárbara Marques

UNIVERSIDADE DE ÉVORA

Título: A fragmentação durante a formação primordial estrela

Resumo:

Compreender os mecanismos físicos que são responsáveis pela formação e evolução das primeiras estrelas do universo, conhecidas como estrelas de população III (ou Pop II) é fundamental para compreendermos como evoluiu o universo até hoje. No modelo padrão da formação de estrelas de Pop III, a matéria bariónica é constituída principalmente por hidrogénio atómico na forma gasosa, e colapsa gravitacionalmente em mini-halos (pequenos halos) de matéria escura, dando origem à formação das estrelas. No entanto, muito pouco se sabe como a evolução dinâmica e química do gás primordial são afetadas pelas condições iniciais dos mini-halos, em particular no que diz respeito ao efeito da rotação nos aglomerados estelares instáveis que se formam dentro dos mini-halos, ao impacto da turbulência, à formação de hidrogénio molecular, e ao impacto das variações cósmicas entre mini-halos.

Neste trabalho usamos uma versão modificada do código Gadget-2, um programa de simulação hidrodinâmica baseado num algoritmo numérico conhecido por SPH (“smoothed particle hydrodynamics”), que permite seguir a evolução do gás durante o colapso, tanto no caso de mini-halos idealizados como em casos de mino-halos mais realistas. Em contraste com algumas simulações numéricas mais antigas, a implementação das partículas coletoras (“sink particles”) permite seguir a evolução do disco de acreção que se forma no centro dos fragmentos e dos mini-halos.

Descobrimos que o processo de fragmentação depende do valor adotado para a taxa de formação (“three-body H2 formation rate”) de hidrogénio molecular (H2). Verificamos que o aumento da taxa de arrefecimento durante o período em que o hidrogénio atómico é convertido em hidrogénio molecular é compensado pelo aquecimento causado pela contração do gás. Propomos que o arrefecimento de H2, o aquecimento devido a formação de H2, e o aquecimento devido à compressão do gás, juntamente com a densidade e temperatura determinam a estrutura do disco que favorece a fragmentação. Também descobrimos que a rotação inicial da nuvem de gás tem um impacto muito relevante na evolução térmica e dinâmica do gás em colapso.

Nuvens com uma elevada rotação apresentam filamentos idênticos a braços espirais que se tornam gravitacionalmente instáveis, dando origem à fragmentação em várias escalas. Estes tipos de nuvens têm mais tendência a fragmentar e têm menores taxas de acreção em relação a nuvens com menor rotação. Adicionalmente, verificamos que a distribuição especifica de momento angular (L) do gás é descrita por uma relação de potência com a massa do gás capturado (M) dada pela expressão $L = M^{1.125}$. Por sua vez o momento angular é controlado pelo torque gravitacional e pela pressão, embora não dependa dos valores de rotação e turbulência da nuvem inicial.

I certify that I have read this dissertation and that, in my opinion, it is fully adequate in scope and quality as a dissertation for the degree of Doctor of Philosophy.

Signature

I certify that I have read this dissertation and that, in my opinion, it is fully adequate in scope and quality as a dissertation for the degree of Doctor of Philosophy.

Signature

I certify that I have read this dissertation and that, in my opinion, it is fully adequate in scope and quality as a dissertation for the degree of Doctor of Philosophy.

Signature

Approved by Scientific Council Standing Committee of the Institute for Advanced Studies and Research (IIFA), UNIVERSITY OF ÉVORA

Abstract

Understanding the physics of the very first stars in the universe, the so-called Population III (or Pop III) stars, is crucial in determining how the universe evolved into what we observe today. In the standard model of Pop III star formation, the baryonic matter, mainly atomic hydrogen, collapses gravitationally into small Dark Matter (DM) minihalos. However, so far there is little understanding on how the thermal, dynamical and chemical evolution of the primordial gas depend on the initial configuration of the minihalos (for example, rotation of the unstable clumps inside minihalos, turbulence, formation of molecular hydrogen and cosmic variance of the minihalos). We use the modified version of the GADGET-2 code, a three-dimensional smoothed particle hydrodynamics (SPH) simulations, to follow the evolution of the collapsing gas in both idealized as well as more realistic minihalos. Unlike some earlier cosmological calculations, the implementation of sink particles allows us to follow the evolution of the accretion disk that builds up in the centre of each minihalo and fragments. We find that the fragmentation behavior depends on the adopted choice of three-body H_2 formation rate coefficient. The increasing cooling rate during rapid conversion of the atomic to molecular hydrogen is offset by the heating due to gas contraction. We propose that the H_2 cooling, the heating due to H_2 formation and compressional heating together set a density and temperature structure in the disk that favors fragmentation. We also find that the cloud's initial degree of rotation has a significant effect on the thermal and dynamical evolution of the collapsing gas. Clouds with higher rotation exhibit spiral-arm-like structures that become gravitationally unstable to fragmentation on several scales. These type of clouds tend to fragment more and have lower accretion rates compared to their slowly rotating counterparts. In

addition, we find that the distribution of specific angular momentum (L) of the gas follows a power-law relation with the enclosed gas mass (M), $L \propto M^{1.125}$, which is controlled by the gravitational and pressure torque, and does not depend on the cloud's initial degree of rotation and turbulence.

Preface

The knowledge of formation of the very first stars in the universe, also known as Pop III stars, is pivotal for studying the evolution of the universe. The purpose of this work is to investigate the physical mechanisms that affect the evolution of the Pop III star-forming gas clumps. With this aim, we perform a number of smoothed particle hydrodynamics simulations in both idealized as well as more realistic cosmological minihalos using modified GADGET-2 code that include sink particles to represent the contracting protostars. In addition, we investigate the gas evolution with different degrees of solid body rotation, defined as the initial ratio of rotational to gravitational energy, and with different rate coefficients for molecular hydrogen formation.

In this dissertation, we particularly focus on the angular momentum distribution that leads to the development of a gravitationally unstable disk around the initial Pop III stars. The disk then fragments to form a small number of protostars with a range of masses. We methodically investigate the effect of the initial configuration of the gas clump, such as H_2 formation and the strength of rotation, on the fragmentation of the disk. We also explore the possibility of survival of the Pop III stars till today.

Indeed, this is an useful step towards the understanding of the fragmentation behavior of the primordial gas. We believe that this research work will provide a straightforward and meticulous analysis to the 'First stars community' for better understanding of many important issues such as operation of the chemothermal instability, angular momentum distribution and the mass accretion process during the primordial gas collapse in early universe. This preface is just to provide a synopsis of the original research that has been published in peer reviewed journals and described by the candidate in the following chapters.

Acknowledgement

First and foremost, I would like to thank Prof. Manuel Pereira dos Santos, Prof. Ilidio Lopes, Prof. Mourad Bezzeghoud and Prof. Miguel A. de Avillez for providing me a platform to submit thesis in the Institute for Advanced Studies and Research (IIFA), Universidade de Évora. Without their help, initiative and guidance, it would never be possible to reach the final step of the dissertation. I am highly grateful to them for their constant support, communication and nice cooperation. I also thank them for throughly checking the manuscript and for efficacious comments on the thesis. In addition, I sincerely thank the members of the Scientific Council Standing Committee for accepting the thesis for public defense. I express my wholehearted gratitude to Prof. Rui Paulo Salgado, Dr. Joana dos Santos, Dr. Nanda Kumar, Dr. Andrea Nerozzi and Dr. Ana Prates for making the thesis defense successful. I also thank the entire administrative staff of IIFA and Universidade de Évora for their continuous support.

I would like to thank my collaborators Prof. Biman Nath, Dr. Paul Clark, Prof. Ralf Klessen, Prof. John Wise and Dr. Athena Stacy who have been guiding me on various scientific problems throughout the journey. I also acknowledge Prof. Prateek Sharma, Prof. Takashi Hosokawa, Prof. David Sobral, Prof. Sharanya Sur, Prof. Somnath Bharadwaj, Prof. Dominik Schleicher, Prof. Kazu Omukai, Prof. Andrei Mesinger, Prof. Agnieszka Janiuk, Prof. B. N. Dwivedi and Prof. Andrea Ferrara for enormous constructive suggestions and comments on the manuscripts. The research that composes this thesis would not have been possible without the guidance of my collaborators. I thank Dr. Thomas Greif for providing me the data from his simulations, on which some of the calculations is based. All the computations were performed on the HPC-GPU Cluster Kolob (funded by the Heidelberg University).

I acknowledge all those referees and editors of the prestigious journals where we have published the results. Their numerous comments and suggestions have helped us a lot to ameliorate the clarity of the papers. I have been enlightened from the number of suggestions that they have provided during publications.

I started PhD in the Institute of Theoretical Astrophysics of the Center of Astronomy of the Heidelberg University, Germany. During PhD, I had been selected for the 'First Star IV' conference in Kyoto, Japan in 2012, where I was honoured with the best award for the Poster Prize. On same year, I went to Switzerland and Austria to attend the prestigious 'Saas fee course' and winter school. However, during travelling, I have been suffering from cold, which ultimately affected my lungs and heart. I was therefore hospitalised and undergoing treatment for six months in Germany.

Following the suggestions of the doctors, I had to return to India, and was in rest for next three months. Thanks to the Raman Research Institute (RRI) and Indian Institute of Science (IISc), which have provided me an opportunity to complete the thesis work. I have high respect for the director of RRI, Prof. Ravi Subrahmanyan, who granted me with the research fellowship and local hospitality. A significant part of the thesis has been carried out in RRI under the guidance of Prof. Biman Nath, who has supervised me on our first publications and has been a 'role model' for me to follow. I also sincerely thank Vidya for helping me with the administrative issues. The second part of the thesis has been carried out in IISc, where I was supported from the personal grant of Prof. Banibrata Mukhopadhyay and Prof. Prateek Sharma. I am indebted to Prof. Banibrata Mukhopadhyay, who has been assisting me continuously throughout my PhD journey.

To finish the rest of thesis, I have visited a number of institutions in India such as Inter-University Center for Astronomy and Astrophysics (IUCAA) at Pune, Indian Institutes of Technology – Kharagpur (IIT–KGP) and Department of Physics of the Indian Institute of Technology–Banaras Hindu University (IIT–BHU) at Varanasi. These institutions have always arranged accommodation, hospitality and travel allowance for my visit. A heartfelt thanks to all the professors who have invited me as their guest to help me complete the thesis, to name some of them, Prof. Kandaswamy Subramanian and Prof. Neeraj Gupta from IUCAA, Prof. Debaprasad Giri and

Prof. Sandip Chatterjee from IIT-BHU, Prof. Somnath Bharadwaj and Prof. Sayan Kar from IIT-KGP and Prof. Shiv Sethi from RRI. I also thank Prof. Andrei Mesinger for granting me a visit for three months to Scuola Normale Superiore at Pisa, Italy.

The initial phase of the thesis work was supported by the Germany government, Landesstiftung *Baden-Württemberg Stiftung* under grant P-LS-SPII/18 'Formation of the First Stars'. Furthermore, the work is partially supported by the Indian Space Research Organization (ISRO) grant (No. ISRO/RES/2/367/10-11) and Department of Science and Technology (DST) grant (Sr/S2/HEP-048/2012). In addition, I am appreciative to the Centre for Theoretical Studies (CTS) at the IIT–KGP for the financial support and hospitality.

I should express my unfeigned gratitude to my friends–they are simply exemplary and praiseworthy. My wholehearted thank to my friends for making me smile and laugh even in the toughest moments. They have always been with me all the way. To name a few - Gautam, Debangsu, Kartick, Saurabh, Viral, Kanhaiya, Anirbanda, Lijo, Soumitrada, Abir, Upasana, Bidya, Sujit, Debanjan, Siddhartha, Anjan, Soumya, Samir, Aminur, Nirmalendu, Sampath, Narayan, Debasish, Abhishek Kumar, Abhishek Dubey, Reju, Jenny, Anasua, Avik, Santanu, Santi, Arka, Ramu, Manu, Tarak, Kaustubh Vaghmare, Swagat, Vivek da, Gautam da, Prof. Sudeshna Sinha, Prof. Jose Afonso, Prof. Rolf Kuiper and Mr. Kulasingam Rasaratnam – thank you everyone for being there with me while I was dealing with any kind of troubles, frustration or financial problem. You people deserve my love and respect.

I would like to thank my parents, sister and relatives for supporting me in whatever I please to do and encouraging me to always try my best. I would also like to thank the Satsang Community in Bangalore and Pune. Spending time with Gurubhais and activities during the construction of 'Mandir' have always given me immense pleasure. I have been associated with the Satsang Bihar for long time. The more I follow and practice the ideology of my 'Guru' Sree Sree Thakur Anukul Chandra, the founder of the Satsang, the more I realise the self-control against my own complexities, mental support, boost and patience. I got the spirit of 'never to give up–fight till the end'. Most importantly, I have always enjoyed attending the Satsang. Finally, I thank my 'Guru' Sree Sree Thakur and reverent 'Thakur family' for their blessing.

List of Publications

Publications for this Dissertation

1. **Jayanta Dutta**
   "Angular momentum evolution during gravitational collapse of primordial star forming clouds",
   Astrophysics and Space Science, **Letter**, 361:35, January 2016

2. **Jayanta Dutta**
   "On the effects of rotation in primordial star-forming clouds",
   Astronomy & Astrophysics, Volume 585, A59, January 2016

3. **Jayanta Dutta**
   "Does the Chemothermal Instability Have Any Role in the Fragmentation of Primordial Gas",
   The Astrophysical Journal, Volume 811, Issue 2, 98D, 2015

4. **Jayanta Dutta**, Biman B. Nath, Paul Clark and Ralf Klessen
   "The role of three-body H_2 formation in the fragmentation of primordial gas",
   MNRAS, Volume 450, Issue 1, p.202-208 (2015)

5. **Jayanta Dutta** et al.
   "On the effects of rotation during the formation of population III protostars",
   AIP Conference Proceedings, Volume 1480, pp. 333-336 (2012) (Best Poster Prize)

Other Publications

1. **Jayanta Dutta**, G. Ananthakrishna and S. Banerjee
   "On the athermal nature of the β to ω transformation",
   Acta Materialia, Volume 60, Issue 2, pp. 556-564 (January 2012)

2. Bidya Binay Karak, **Jayanta Dutta** & Banibrata Mukhopadhyay
   "Search for Chaos in Neutron Star Systems: Is Cyg X-3 a Black Hole?",
   The Astrophysical Journal, Volume 708, Issue 1, pp. 862-867 (2010)
   The Astrophysical Journal, Volume 715, Issue 1, pp. 697 (2010), Erratum

Contents

List of Tables

List of Figures

Chapter 1

Introduction

Understanding of how the universe was formed has always been the subject of great interest. In the last century, there were a number of pioneering works in this field, for example, formulation of general relativity and prediction of gravitational waves by Albert Einstein in 1916, Georges Lemaître's hypothesis for the expansion of the universe in 1927 followed by Edwin Hubble's first observational basis in 1929 that galaxies in all directions are receding from us, to name a few. The unexpected detection of the Cosmic Microwave Background (CMB: Penzias & Wilson 1965; Dicke, Peebles, Roll & Wilkinson 1965) yields a boost to the observational cosmology because it is the oldest light in the universe imprinted on the sky (Preliminary results from the COBE: Mather et al. 1990; Smoot et al. 1991). These discoveries along with many other groundbreaking theoretical as well as observational studies have provided a great stride in our understanding of the overall physical content of the universe, which is believed to be expanding as well as accelerating (Riess et al. 1998; Perlmutter et al. 1999). The advent of state-of-the-art telescopes and satellites such as the Spitzer Space Telescope (SST), Hubble Space Telescope (HST), Chandra X-Ray Space Telescope, Planck and high resolution numerical simulations such as 'Millennium Simulation' (Springel et al. 2005) and other Eulerian as well as Lagrangian codes have provided a robust insight into the history of the universe in which we now live. Therefore, how the distribution of matter in the universe has evolved over time and how the observed population of galaxies was formed are the final frontiers in modern astrophysics and cosmology.

According to the Big Bang model, the universe in its initial stage was fairly homogeneous (e.g., Barkana & Loeb 2001; Miralda-Escudé 2003). In the context of the ΛCDM model, where Λ is the cosmological constant that is associated with dark energy and cold dark matter (CDM), studies show that the hierarchical structure formation eventually leads to the collapse of the first gravitationally and thermally unstable primordial gas clouds (see e.g., Yoshida et al. 2003; Reed et al. 2005; Ciardi & Ferrara 2005). The very first stars in the universe, the so called Population III (or Pop III) stars, are believed to have formed only a few hundred million years after the Big Bang (Abel, Bryan & Norman 2002; Bromm & Larson 2004; Glover 2005), thus ending the 'cosmic dark ages' (Yoshida et al. 2006; O'Shea & Norman 2007). This era marks a crucial transition from the simple universe to the present-day clumpy state, where we can see innumerable stars, galaxies and other objects (Wise & Abel 2008; Bromm, Yoshida, Hernquist & McKee 2009; Loeb 2010). The large-scale high-resolution simulations provide a complicated structure of turbulent gas and supernova-driven interstellar medium (ISM e.g., de Avillez Miguel et al. 2012; Hirano & Yoshida 2013; Greif 2014; Klessen & Glover 2015).

The ultraviolet radiation from first generations of stars heated and ionized the pristine intergalactic medium (IGM), heralding cosmic reionization (e.g., Kitayama et al. 2004; Mesinger, Johnson & Haiman 2006; Abel, Wise & Bryan 2007). Reionization lifted the cosmic fog, allowing visible light to finally spread throughout space (Whalen et al. 2008; Loeb & Wyithe 2008). Recent observations using carbon as a tracer of metals have shown that Pop III supernovae can be significant contributors to the very low overdensity Lyα forest (Schaye et al. 2003; Frebel et al. 2005). Therefore it is believed that some of these stars produced the supernovae (SNe) explosions and released the first heavy elements into the IGM (e.g., Madau, Ferrara & Rees 2001; Heger & Woosley 2002; Schneider et al. 2003; Norman, O'Shea & Paschos 2004). Other studies show that perhaps the first stars set the stage for the next stellar generations, and it was the later generations that produced the metallicity (Omukai et al. 2005; Schneider et al. 2006; Tornatore et al. 2007). The first stars fundamentally altered the chemical and thermal state of the gas out of which the first galaxies formed (Mac Low & Ferrara 1999; Oh & Haiman 2002; Wada & Venkatesan 2003). The

study of the first stars has also enhanced our understanding of the high-redshift observations of quasars (Maiolino et al. 2004; Venkatesan et al. 2004; Furlanetto & Mesinger 2009) and nature of the dark matter halo (Lopes et al. 2011; Lopes & Silk 2014). Therefore, the knowledge of the evolution and properties the first generation of stars is essential in comprehending the history of the universe.

1.1 Basics of Pop III star formation

Over the course of last three decades, studies by a number of groups have led to the development of a widely accepted standard model of primordial star formation. In this picture, the very first protostars form within small dark matter (DM) halos that have a virial temperature of ∼1000 K and masses of $\sim 10^5$–$10^6 M_\odot$, and which collapse at redshift $z \geq 20$ (see, e.g., Haiman et al. 1996; Tegmark et al. 1997; Bromm, Coppi & Larson 1999). The baryonic matter, mainly the atomic hydrogen and helium that combines the gas, gravitationally falls into the potential well of DM halos, and undergoes heating as well as a series of chemical reactions, which enhances its molecular hydrogen (H_2) abundance allowing the gas to cool more efficiently and collapse (Glover & Abel 2008; Glover & Savin 2009).

Unlike in contemporary star-forming gas clumps, primordial gas has no metals to provide rapid cooling. The importance of H_2 for the cooling of low-mass gas clumps that condense out of the expanding universe was recognized in the late 1960's (Saslaw & Zipoy 1967; Peebles & Dicke 1968; Silk 1977; Couchman & Rees 1986). Using simplified one-zone models these pioneering works have provided the basis for the subsequent one-dimensional calculations (e.g., O'Shea & Norman 2008) and three-dimensional simulations of collapse of the primordial gas (e.g., Abel, Bryan & Norman 2000, 2002; Bromm, Coppi & Larson 2002; Yoshida, Omukai & Hernquist 2008).

1.1.1 Initial gas collapse

The hydrogen atoms (H) combines with free electrons (that is present in the gas from the epoch of cosmological recombination at $z \sim 1100$) to form H^- as an intermediate

state, which in turn combines with H to produce H_2 and an electron. In this way electrons act as catalysts. Theoretical calculations show that the fractional abundances of H_2 (denoted by x_{H_2}) is quite small, $x_{H_2} \sim 10^{-3}$ (Susa et al. 1998; Yoshida et al. 2003). As the collapse proceeds, the gas is cooled via H_2 rotational and vibrational line emission (also termed as gas-phase reaction), with H^- ion as an intermediate state (first discussed in the context of the local ISM by McDowell 1961)

$$H + e^- \rightarrow H^- + \gamma, \tag{1.1}$$

$$H^- + H \rightarrow H_2 + e^-, \tag{1.2}$$

where the free electrons act as catalysts (Omukai & Nishi 1998). At this point, gas attains a temperature ∼200 K that depends upon the dynamical history of the collapse. This minimum temperature is reached at a density of around 10^4 cm^{-3} and is comparable to the critical density of H_2 (i.e., the density at which its level populations reach their local thermo-dynamical equilibrium (LTE) values). However, the limited H_2 abundance is not sufficient to cool the gas further, and the gas begins to heat up adiabatically with increasing density. This results in the free-fall time being shorter than the cooling time. The transition from the cooling (low density) to heating (high density) with increasing density occurs near this critical density $n_{cr} \approx 10^4$ cm^{-3}, and sets a characteristic Jeans length, allowing the gas to fragment with the Jeans mass, M_J (Bromm & Larson 2004), defined as

$$M_J \approx 700 M_\odot \left(\frac{T}{200\ \mathrm{K}}\right)^{3/2} \left(\frac{n}{10^4\ \mathrm{cm}^{-3}}\right)^{-1/2}. \tag{1.3}$$

At higher density (∼10^7–10^8 cm^{-3}) hydrogen molecules are formed by the three-body reactions (Palla, Salpeter & Stahler 1983):

$$H + H + H \rightarrow H_2 + H, \tag{1.4}$$

$$H + H + H_2 \rightarrow H_2 + H_2. \tag{1.5}$$

There is however a significant uncertainty in the rate coefficients for the above set

of reactions that can cool the gas rapidly by converting almost all the atomic hydrogen into molecules, making the gas chemothermally unstable (Turk, Abel & O'Shea 2009). In addition, the sudden formation of H_2 has two interesting effects. The formation of H_2 is accompanied with the release of binding energy (4.4 eV), which then heats the gas. Therefore, if the three-body H_2 formation rate is fast enough, the resulting heating can momentarily stall the collapse. Simultaneously, once the H_2 molecule forms, this can cool the gas.

Moreover, the amount of H_2 molecules produced is a strong function of temperature. At high temperature, H_2 molecules are destroyed by collisions with atomic H and H_2 molecules (Yoshida et al. 2006),

$$H_2 + H \rightarrow H + H + H, \tag{1.6}$$

$$H_2 + H_2 \rightarrow H + H + H_2. \tag{1.7}$$

The collision dissociation of H_2 prevents the fractional abundance (x_{H_2}) from becoming large. The study by Turk et al. (2011) has discussed the equilibrium condition between the abundances of atomic and molecular hydrogen, known as the principle of microscopic reversibility. So, the rate at which H_2 is produced via the three-body reaction must be compensated by the destruction rate to bring the system to a chemical and thermal equilibrium. In LTE, the adopted values of the rate coefficient for the H_2 collisional dissociation ($k_{\rm diss}$) must be consistent with the three-body formation rate coefficient ($k_{\rm form}$) in the sense that each pair of rate coefficients satisfies the chemical equilibrium condition $k_{\rm form}/k_{\rm diss} = K$, where K is the equilibrium constant.

1.1.2 Gas evolution to protostellar densities

Once the gas density reaches a value $\sim 10^{10}$ cm^{-3}, the cloud becomes optically thick to the strongest of H_2 lines. In the high-density regime ($\sim 10^{14}$ cm^{-3}), the gas goes through a phase of cooling instability due to a strong increase in the cooling rate by H_2 collisional induced emission (CIE; Ripamonti & Abel 2004). Above the central density $\sim 10^{16}$ cm^{-3}, the gas becomes completely optically thick to the continuum radiation

(Yoshida, Omukai & Hernquist 2008). At this point the remaining H_2 dissociates via reactions (1.6, 1.7), and hence cools the gas to collapse further. Once all the H_2 dissociates, the gas becomes fully adiabatic with core mass $\sim 0.01 M_\odot$ surrounded by a massive, dense envelope that accretes matter rapidly (Clark et al. 2011a).

Early simulations show the formation of massive primordial protostars ($\sim 100 M_\odot$) once the central density reaches $\sim 10^{16}$ cm^{-3} (Abel, Bryan & Norman, 2000; Yoshida et al., 2006). However, the final masses of the protostars depends on the accretion rate as well as dynamical history of the collapse, and lies anywhere between $\sim$10–$1000 M_\odot$ (O'Shea & Norman 2007). The study by McKee & Tan (2008) shows that the radiative feedback from dense core, mainly Ly-α scattering and photoionization, can prevent the accretion process, thereby leaving the final mass of protostars completely uncertain. Recently, the radiation-hydrodynamics simulation by Hosokawa et al. (2011) shows that the ultraviolet (UV) radiation from the protostars can suppress the accretion and destroy the circumstellar disk completely. The strength of the UV radiative feedback depends on the stellar luminosity and effective temperature, and protostars can ultimately grow to $\sim 40 M_\odot$. Similar studies show that the mass accretion onto Pop III protostars is significantly suppressed by their radiative feedback, resulting in the formation of small multiple systems having final masses in the range $\sim$1–$60 M_\odot$ (Susa 2013). Hence the evolution of central protostar and its final mass significantly depends on the accretion process and radiative energy loss from the stellar interior.

1.2 Disk Fragmentation

As the collapse proceeds to higher density, gas particles continually fall onto the central core, heralding the accretion disk around it to become more and more unstable. It has been shown that the collapsing gas can fragment into distinct parts, each evolving independently to form its own protostar (Turk, Abel & O'Shea 2009). The possible mechanisms for the disk to fragment are gravitational instability (Larson 1969), turbulence (Abel et al. 1998) or thermal instability (Omukai & Yoshii 2003). Gravitational instability is also important for angular momentum transport and energy dissipation in a self-gravitating accretion disk within local viscous frame (Lodato & Rice 2004).

Recent improved numerical simulations use 'sink particle method' (a computational technique to represent the growing protostar, discussed in the subsequent chapters) to propose that the disk around the first protostar exhibits spiral structure that develops nonaxisymmetry features and becomes locally unstable within few hundred years after the first star is formed (Stacy, Greif & Bromm 2010). The gravitationally unstable disk then splits into a binary and higher-order systems, which has separations as small as the distance between Earth and the Sun, instead of a single protostar as proposed in earlier studies (Clark et al. 2011). These multiple unstable clumps can accrete the surrounding gas and form secondary protostars. However, protostars that form in the disk fragmentation have small masses (Greif et al. 2011; Smith et al. 2011). The surface density remains roughly constant as the disk evolves, with the temperature behaving in a similar fashion. The amount of the gravitational instability of the disk can be measured by the Toomre Q-parameter, defined as

$$Q \equiv \frac{c_s \kappa}{\pi G \Sigma}\,, \tag{1.8}$$

where c_s is the sound speed, κ is the epicyclic frequency, G is the gravitational constant and Σ is the surface density. If we consider the disk to be Keplerian, the epicyclic frequency can then be replaced by orbital frequency, $\kappa_{\rm Keplerian}$, where, $\kappa_{\rm Keplerian} = \Omega = \sqrt{GM(r)/r}$. Here $M(r)$ is the mass enclosed within the radius r. If the value of the parameter, Q, is larger than 1, the disk remains stable against collapse, whereas, for $Q < 1$ the disk becomes unstable. For $Q \sim 1$, the disk are dominated by gravitational instabilities and fragments. The outer disk continually builds up more and more mass, thus the Q-parameter remains around 1 in the outer region (Clark et al. 2011).

The fragmentation of disk has significant implications on the final masses of the first stars, which is still a debate among the researchers. The ultimate goal of the study of Pop III gas collapse is to determine the mass function for the very first stars in the universe. Models of single-protostars suggest a vast range of masses $\sim$10–1000$M_\odot$ (Hirano et al. 2014), which is determined by the accretion physics and radiative process. On the other hand, if the disk around first stars fragments due to gravitational instability, the characteristic masses may be much smaller, similar to the present day

star formation (Kroupa 2002; Chabrier 2003). Theoretical calculations show that there is possibility of finding Pop III stars in the present-day local universe provided they were formed as low mass stars $\leq 0.8M_{\odot}$ (Greif et al. 2011; Susa 2013). The mass of the star also determines its luminosity, ionizing photon production (Tumlinson & Shull 2000) and whether the stars die as metal-ejecting supernovae or collapse into black holes. Therefore, to understand the overall impact of Pop III stars on the early universe, we must better understand the initial mass function (IMF) of the first stars.

1.3 Problems to be discussed in this thesis

In this dissertation, we particularly focused on the disk fragmentation that occurs after the formation of first protostar. Fragmentation may depend on various issues such as thermal and chemical history of the collapse, interaction with the surroundings, gas mass and instability in clouds. However, the degree to which the disk fragments depends on the initial properties of halos (e.g., chemical abundances, initial rotation, turbulence, cosmic variance) has never been systematically tested. Using idealized numerical experiments, previous studies (e.g., Machida et al. 2008; Saigo, Tomisaka & Matsumoto 2008) show that the resulting disk fragmentation depends on the cloud's initial strength of rotation. However, their calculations were restricted by the equation of state (EOSs), and so, could not self-consistently follow the thermal, dynamical and chemical evolution of gas. Besides, these studies did not include sink particles, and therefore could not investigate the fragmentation of disk.

In addition, there are open questions such as how the angular momentum is continually distributed during star formation (Larson 1969, 1972; Silk 1977; Norman, Wilson & Barton 1980). There are indications that the collapsing clouds from which the protostars form could have a strong rotational support (Couchman & Rees 1986; Bodenheimer 1995). A number of studies show that the angular momentum of a single star or star-cluster is much lower than that of the original cloud in which the protostars form (O'Shea & Norman 2008; Turk, Abel & O'Shea 2009). So the question remains of how the collapsing cloud redistributes the excess angular momentum and why the distribution follows a characteristic power-law behavior, which has been shown

in many cosmological simulations (Abel, Bryan & Norman 2002; Bromm, Coppi & Larson 2002). In case of present-day star formation, the distribution is controlled by the magnetized stellar winds and magnetic braking (Matt et al. 2010). For primordial collapse, the actual process of redistribution is still ambiguous and of utmost interest.

Moreover, the physical process at high densities ($\sim 10^7$–10^8 cm^{-3}) is extremely complex (Omukai & Nishi, 1998) and is relevant to the inception of the thermal instability that may promote the gas to fragment (e.g. Omukai & Yoshii 2003; Yoshida, Omukai & Hernquist 2007; Greif, Springel & Bromm 2013). During the three-body H_2 formation reaction, there is concurrent process of heating and cooling. For example, rapid formation of the molecular hydrogen cools the gas and simultaneously releases the binding energy that can heat the gas. On the other hand, continuing collapse contributes to the compressional heating (pdV). The physics of gas collapse at high densities therefore becomes extremely complicated. There is, however, little understanding of how the three-body H_2 formation reaction can regulate the heating and cooling process during collapse, thereby affecting the disk fragmentation.

With the help of improved numerical simulations (e.g., smoothed particle hydrodynamics code GADGET-2 by Clark et al. 2011a and moving mesh code AREPO by Greif et al. 2011), we attempt to address important issues such as heating and cooling rates during the crucial three-body reactions, onset of chemothermal instability and distribution of the angular momentum while describing the velocity structure, accretion rate and temperature evolution of the primordial gas in both the idealized as well as more realistic cosmological minihalos. In particular, we focus on how the initial conditions of the collapsing gas clumps can modulate the thermo-dynamical evolution and thus provide a hint of future fragmentation of disk.

1.4 Objectives and milestone

Much excellent efforts have already been made by a number of groups to understand the gas evolution till the protostellar density. However, there have been so far few studies on the issues of disk fragmentation. With a growing knowledge of Pop III gas collapse and with improved numerical simulations, including the work described in

the following chapters, we hope to achieve an insight into the fragmentation behavior.

The aim is to understand better the physical process that can promote the resulting fragmentation of disk. To achieve this, we first, in particular, need to understand how the angular momentum distribution of gas ultimately leads to the formation and build-up of the disk. In this process, we should be able to address many important aspects such as the accretion physics, velocity structure, temperature evolution and heating and cooling processes.

The next step is to investigate in detail the relation between the fragmentation behavior and initial configurations of the collapsing gas clumps. For example, how does the instability in the gas vary with the initial rotation of the gas clumps? What is the mass accretion rate of the protostars? Does it depend on the initial angular momentum? In addition, we have noticed in §1.1 that the three-body H_2 formation reaction is crucial for the thermal evolution of the gas. One of the important issues is to investigate the effect of the rate co-efficients of molecular hydrogen formation on the instability in the gas clumps, which can then promote the disk fragmentation. These are the essential questions to address while simulating the primordial gas collapse. Moreover, we can estimate the possibility of the survival of the primordial protostars until the present day. In this dissertation we hope to study these key aspects during the formation and evolution of the Pop III stars.

1.5 Outline

We take care to ensure that our calculations should not be biased on the choice of minihalos. We therefore use two completely different numerical setups: minihalos from the cosmological simulations and artificial minihalos with an initially uniform density distribution of gas particles. Our modified GADGET-2 simulations includes sink particles, which allows us to follow the evolution of the gas beyond the point at which the first protostar forms and to capture the fragmentation. In additional, we use the network for primordial hydrogen, helium and deuterium chemistry to model the chemical and thermal evolution of the gas. However, our model excludes the effect of the magnetic fields, the background radiation or metals produced by stars in other

minihalos, and thus describes star formation in truly pristine primordial gas. The dissertation is organized in the following manner.

In **Chapter 2**, we investigate the role of three-body H_2 formation rate on the resulting fragmentation behavior of the gas (Dutta, Nath, Clark & Klessen 2015). The three-body H_2 reactions that happen in the high density regime $n \sim 10^8$–10^{10} cm^{-3} are crucial stage of collapse in which almost all the atomic hydrogen rapidly converts into molecular form. This allows the gas to cool very efficiently. However, the rate coefficients are uncertain by two orders of magnitude. We focus on the effects of the three-body reaction rate coefficient on the fragmentation of primordial gas.

In **Chapter 3**, we extend the study to understand in detail the chemothermal instability and the associated physical processes during the three-body reaction, in which the gas can cool faster than the free-fall time ($t_{\rm cool}/t_{\rm ff} < 1$). We compare different kinds of heating and cooling rates and discuss their roles in the long-term evolution of the disk that fragments into several clumps. We find that the sum of all the cooling rates is less than the total heating rate after including the contribution from the compressional heating (Dutta 2015).

In **Chapter 4**, we perform, for the first time to the best of our knowledge, a systematic study of the role of initial rotation of the clouds on the resulting fragmentation. The cloud's initial degree of rotation has a significant impact on the heating and cooling process and thus introduces a substantial difference in the Jeans mass, which controls the fragmentation. In addition, we perform rigorous calculations in both the idealized as well as more realistic cosmological minihalos to analyze the physical properties of the gas. We also discuss the possibility of survival of Pop III stars until today (Dutta et al. 2012; Dutta 2016a).

In **Chapter 5**, we discuss the angular momentum evolution during Pop III collapse, which is one of the fundamental problems in the theory of primordial star formation. In particular, we examine how the angular momentum is distributed during collapse. We also discuss the plausible mechanisms for the distribution that is independent of the cloud's initial degree rotation and turbulence (Dutta 2016b).

In **Chapter 6**, we summarize the work described within this dissertation, and draw our conclusions with a brief outlook for future studies.

Chapter 2

The role of three-body H_2 formation in the fragmentation of primordial gas

It has been shown that the behavior of primordial gas collapsing in a dark matter minihalo can depend on the adopted choice of three-body H_2 formation rate. The uncertainties in this rate span two orders of magnitude in the current literature, and so it remains a source of uncertainty in our knowledge of Population III star formation. Here, we investigate how the amount of fragmentation in primordial gas depends on the adopted three-body rate. We present the results of calculations that follow the chemical and thermal evolution of primordial gas as it collapses in two dark matter minihalos. Our results on the effect of three-body rate on the evolution until the first protostar forms agree well with previous studies. However, our modified version of the SPH GADGET-2 code includes sink particles, which allows us to follow the initial evolution of the accretion disk that builds up on the centre of each halo, and capture the fragmentation in gas as well as its dependence on the adopted three-body H_2 formation rate. We find that the fragmentation behavior of the gas is only marginally affected by the choice of three-body rate co-efficient, and that halo-to-halo differences are of equal importance in affecting the final mass distribution of stars.

2.1 Introduction

According to the standard model of the primordial star formation process, the very first stars, the so-called Population III (or Pop III) stars form within dark matter (DM) halos with virial temperature ∼1000 K and masses ∼10^6 $M_\odot$ that collapsed at redshift $z \sim$ 25-30 or above (Haiman et al. 1996; Tegmark et al. 1997; Abel, Bryan & Norman 2002; Glover 2005; Bromm & Larson 2004; Bromm, Yoshida, Hernquist & McKee 2009). The hydrogen atoms in the DM halos combine with the small abundances of free electrons via $H + e^- \rightarrow H^- + \gamma$, followed by $H^- + H \rightarrow H_2 + e^-$, where the free electrons act as catalysts and are present as residue from the epoch of recombination at $z \sim 1100$ (Barkana & Loeb 2001; Ciardi & Ferrara 2005).

The typical fractional abundances of H_2 of ∼10^{-3} are sufficient to permit the primordial gas in the minihalos to cool as it collapses (see, e.g., Susa et al. 1998; Yoshida et al. 2003) via H_2 rotational and vibrational line emission. This occurs until the gas reaches a temperature ∼200K (Omukai & Nishi 1998) at a density of ∼10^4cm^{-3}, at which point the H_2 energy levels move into the local thermodynamical equilibrium (LTE) with the kinetic temperature of the gas, and the resulting cooling time becomes longer than the free-fall of the gas. The gas now heats up slightly as the collapse proceeds. This transition from cooling to heating with increasing density sets a characteristic Jeans length, allowing the gas to fragment with Jeans mass of $M_\mathrm{J} \sim 1000 M_\odot$ at typical temperatures of $T \sim 200\,\mathrm{K}$ and number densities $n \sim 10^4\,\mathrm{cm}^{-3}$ (Abel et al. 1998; Abel, Bryan & Norman 2002; Bromm, Coppi & Larson 1999, 2002).

Once the gas reaches a number density of ∼10^8cm^{-3}, further H_2 formation is possible via the three-body reactions 1.4,1.5(Palla, Salpeter & Stahler 1983). Unfortunately, the rate coefficients for the above set of reactions are very uncertain in the temperature regime which is applicable to Pop III star formation, with the current estimates in the literature spanning two orders of magnitude (see Glover & Abel 2008; Glover & Savin 2009 for discussion). However, independent of the choice of rate coefficient, calculations of the gravitational collapse of primordial gas show that by a number density of ∼10^8cm^{-3}, almost all the atomic hydrogen is converted to H_2 (Yoshida et al. 2006; Turk, Abel & O'Shea 2009).

The sudden formation of H_2 has two interesting effects. First, the process is accompanied by heating, since 4.4 eV is released for every H_2 molecule that is formed. If the formation rate is fast enough, this heating can momentarily stall the collapse against collapse. On the other hand, the ability of the gas to cool is proportional to (among other things) the fractional abundance of H_2, so the more H_2 is formed, the more the gas can cool. In practise, the interplay between these two phenomena is complex, and depends crucially on the adopted rates for the three-body reactions (Turk et al. 2011). Under certain conditions, a chemothermal instability can also occur that may promote the gas to fragment (Yoshida, Omukai & Hernquist 2007; Greif, Springel & Bromm 2013).

In addition to any fragmentation induced by the chemothermal instability, recent simulations conclude that the disk around the first primordial protostar becomes gravitationally unstable and forms a multiple system with low-mass protostars instead of a single protostar (Clark, Glover & Klessen 2008; Stacy, Greif & Bromm 2010; Clark et al. 2011; Greif et al. 2011; Smith et al. 2011; Dopcke et al. 2013). This can occur on time-scales as short as 10–100 years after the formation of the first object. Clark et al. (2011) show that the fragmentation of this disk results from the fact that the disk is unable to accrete onto the protostar faster than it accretes from the in-falling envelope.

The study by Turk et al. (2011) used both smoothed particles hydrodynamics (SPH) and adaptive mesh refinement (AMR) simulations to conclude that the choice of three-body-rate coefficients can introduce significant uncertainty into the radial velocity, temperature and accretion rate, and therefore can affect the rate at which the protostellar disk is fed. This has recently been verified by Bovino, Schleicher & Grassi (2014), who used both old rates and newly calculated improved rate given by Forrey (2013), to reach similar conclusion as Turk et al. (2011). Although they found compressed spiral arms, with strong density contrast between the arms and embedding medium, these simulations were unable to follow the evolution beyond the formation of the protostar, and so could not address the long-term behavior of the disk structure.

However the degree to which the disk fragmentation depends on the chemical uncertainties in the three-body H_2 formation rate has never been systematically tested. Previous studies did not include sink particles, and could not study the fragmentation that occurs once the first object is formed. In this work we focus on the effect that the choice of three-body reaction rate has on the fragmentation of the primordial gas.

2.2 Numerical Methodology

2.2.1 Simulation setup

We investigate two minihalos obtained from the cosmological simulations of Greif et al. (2011, 2012), which used the hydrodynamic moving mesh code AREPO (Springel 2010). We use the snapshots from these simulations at a point when the central number density is just below 10^6 cm^{-3} – comfortably before the onset of the three-body reactions – as the starting point for this project. Interpreting the mesh-generating points of AREPO as Lagrangian fluids particles, we then use the AREPO output as the initial conditions for our GADGET-2 (Springel 2005) implementation. The modifications to the standard GADGET-2 include a time-dependent chemical network for primordial gas, and a sink particles to capture the formation of collapsing protostellar cores (Bate, Bonnell & Price 1995; Jappsen et al. 2005). A fuller description of the code and its features can be found in Clark et al. (2011a). The conversion from moving mesh to SPH formalism is the same as that performed by Smith et al. (2011), and indeed the minihalos are identical, both in terms of the baryonic and DM content.

The original AREPO simulations resolve the Jeans length with 128 cells (Greif et al. 2011), at which point further refinement is deactivated, resulting in roughly constant mass particles within central ≈1000 AU. However, to investigate the effect of three-body H_2 reactions, here we use the intermediate AREPO snapshots (when the central number density $n \leq 10^6$ cm^{-3}) as the starting point. Although the initial size of the minihalos are ≈3 pc, all the fragmentation and accretion take place in the central region of the halos where the SPH particle masses are roughly 10^{-4} $M_\odot$. In GADGET-2 simulation the mass resolution for 100 SPH particles (e.g., Bate & Burkert

Table 2.1: Summary of three-body H_2 formation and dissociation rates adopted here.

Ref	Three-body H_2 formation rates, k_{3bh2} ($cm^6\ s^{-1}$)	Temp range
ABN02	$1.3 \times 10^{-32}(T/300)^{-0.38}$	$(T < 300K)$
ABN02	$1.3 \times 10^{-32}(T/300)^{-1.00}$	$(T > 300K)$
FH07	$1.44 \times 10^{-26}/T^{1.54}$	
	H_2 collisional dissociation rates ($cm^3\ s^{-1}$)	
ABN02	$\frac{1.0670825\times10^{-10}\times(T/11605)^{2.012}}{\exp(4.463/T/11605)\times(1+0.2472\ T/11605)^{3.512}}$	
FH07	$1.38 \times 10^{-4} \times T^{-1.025} \exp(-52000/T)$	

1997) is $\approx 10^{-2}\ M_\odot$.

The chemical and thermodynamical treatment of the gas in the AREPO simulations of Greif et al. (2011) is also identical to those in our GADGET-2 implementation for the range of densities that are studied in this paper. More details of the initial conditions for this study are given below.

Of the various rates available in the literature for the three-body H_2 formation reactions, we choose the extreme rate coefficients: the slowest of which is Abel, Bryan & Norman (2002) (hereafter ABN02) alongside that of Flower & Harris (2007) which provides the fastest of the rates (hereafter FH07). We have used the collisional-dissociation rate in the LTE limit as described in Turk et al. (2011). For our SPH calculation we used a temperature-dependent value calculated via the principle of detailed balanced. For the ABN02 runs, data from Orel (1987) are used for low density (and low temperature, $T < 300$ K) cases, and a power law (described in Table 1) for high density and temperatures. For FH07 runs, we used the rates given in Flower & Harris (2007). For the radiative cooling rate, we use Sobolev approximation to calculate it in the optically thick region, as described in detail in Clark et al. (2011a) and Yoshida et al. (2006). Full details of these rates are given in Table 2.1.

2.2.2 Initial Conditions

The simulations with halo1 start with a maximum central cloud number density (n) 10^6cm^{-3}. The initial temperature of the atomic hydrogen is 470K (max) and 60K (min). Halo1 contains $1030 M_\odot$ of gas and 690855 SPH particles. The maximum and minimum mass of SPH particles are 0.16 $M_\odot$ and 1.3 $\times 10^{-4}$ $M_\odot$. This means that the numerical resolution of our simulations for halo1 for 100 SPH particles is 1.3 $\times 10^{-2}$ $M_\odot$. The simulations with Halo2 starts with a maximum n of 10^6cm^{-3}. The initial temperature of the atomic hydrogen is 436K (max) and 54K (min). Halo2 contains $1093 M_\odot$ of gas and 628773 SPH particles. The maximum and minimum mass of SPH particles are $0.05 M_\odot$ and 1.4 $\times 10^{-4}$ $M_\odot$. This means that the numerical resolution of our simulations for halo2 for 100 SPH particles is 1.4 $\times 10^{-2}$ $M_\odot$. With altogether 6 million particles in the simulation, we resolve the halo gas and its velocity structure significantly better than in the SPH models of our previous study (Turk et al. 2011). However, we note that none of the existing numerical calculations are able to fully resolve the turbulent cascade in the halo gas and do justice to the large Reynolds numbers (of 10^9 or above) that characterise the accretion flow (see, e.g., chapter 4 in Klessen & Glover 2015).

Each of the minihalos are simulated with the two contrasting three-body reaction rates, resulting in 4 simulations in total. The different minihalos allow us to distinguish between those features of the high-density collapse (or evolution) that are caused by the chemothermal differences arising from the reaction rates, and those features which result from cosmic variance (i.e., differences caused by the formation of the minihalos).

As collapse progresses in the central region of the cloud, sink particles are created once the number density of the gas reaches 5 $\times 10^{13}$cm^{-3}, at which point the gas has a temperature of around 1000K. The corresponding Jeans mass at this density and temperature is $0.06 M_\odot$, so our calculations for both of the halos are well resolved. We replace a candidate particle by a sink particle (see, e.g., Bate, Bonnell & Price 1995; Krumholz, McKee & Klein 2004; Jappsen et al. 2005) that can accrete gas particles within its accretion radius $r_{\rm acc}$ that we fix at 6 AU, which is the Jeans radius at the density threshold for sink creation. We also prevent sink particles from forming within $2\,r_{\rm acc}$ of one another in order to avoid spurious formation of new sink particles out of

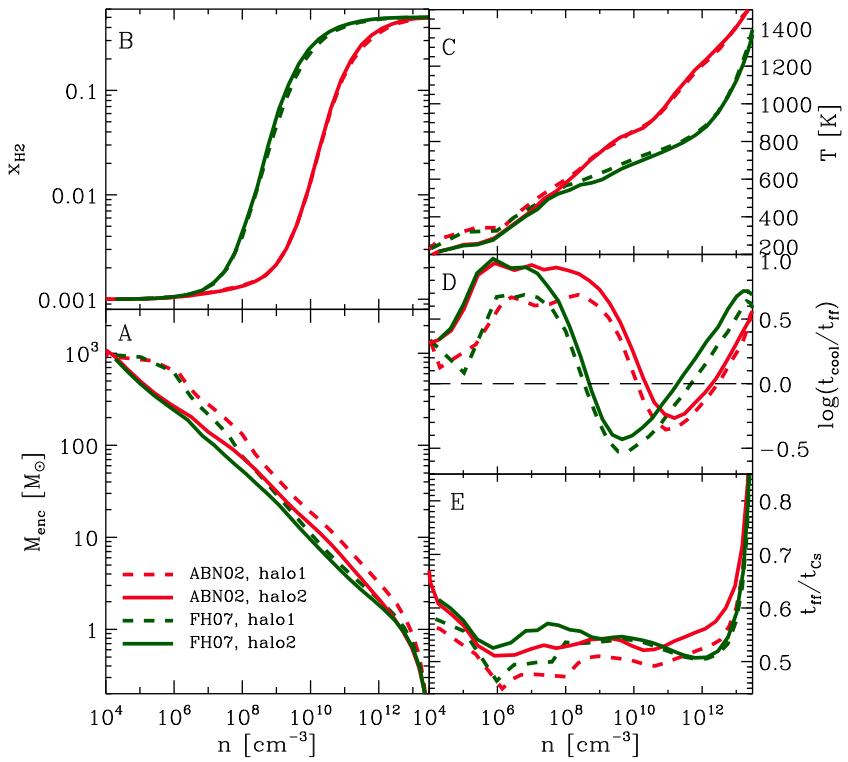

Figure 2.1: Radially binned, mass-weighted averages of physical quantities for different three-body H_2 formation rate (red: ABN02, green: FH07) of two different cosmological halos (dotted: halo1, solid: halo2), are compared just before the first protostar forms. The enclosed mass (A), H_2 fraction (B), temperature (C), ratio of cooling time to free-fall time (D) and ratio of free-fall time to sound-crossing time (E) are plotted as a function of number density.

gas that, in reality, would by accreted by a neighbouring sink particle. Lastly, gravitational interactions between sinks, and between the sinks and the gas, are softened using a fixed softening parameter of 1.2 AU for the sinks. We run our simulations until a mass of 21 $M_\odot$ has been accreted by all the sink particles. The final time scales range between 2500–4000 yr due to the physical differences between the minihalos and the three-body H_2 formation rates.

2.3 Physical conditions just before sink particle creation

In this section we examine the physical conditions in the gas once the central region has collapsed to a density of $\sim 5 \times 10^{13}$ cm^{-3}. The radial profiles of the gas for the two different halos and two different three-body rates are shown in Fig. 3.1. The panels show mass-weighted averages of the properties of individual SPH particles within radial logarithmic bins.

Panel A shows the mass enclosed as a function of the number density, and we see that it displays a rough power-law over most of the density range covered here. This simply follows from the radial power-law in the density which is typical for primordial gas: $n(r) \propto r^{-2.2}$ (e.g., Abel, Bryan & Norman 2002; Yoshida et al. 2006; Yoshida, Omukai & Hernquist 2008). We see that there are slight differences between the profiles for the two rates, but these are also comparable to the differences between the two halos.

In panel B, we see the rapid rise in the H_2 fraction with increasing density that arises from the three-body reactions. Here we see a clear difference between the two rates, with the runs with FH07 producing most of the H_2 by a density of 10^9 cm^{-3}, while the ABN02 runs are only starting to produce H_2 by the time this density is reached. As the rates are a strong function of density, we see very little difference in the H_2 fractions between the two halos.

The mean temperature as a function of the number density is shown in panel C. We find that the gas is significantly cooler, up to a factor of 2, around density $\sim 10^{12}$ cm^{-3}, in the FH07 halos than in those using ABN02. The differences in temperature-density evolution start around a number density of 10^7 cm^{-3}, once the H_2 abundance in the FH07 case has increased by an order of magnitude. Again, we find that there is little difference between evolution of halos 1 and 2 in this panel, implying that the chemical state of the gas is more important for the temperature evolution than any differences in the halo properties. Curves in panels A, B and C are consistent with the results of Turk et al. (2011).

2.4 Velocity structure and accretion

In this section we study the difference in mass accretion associated with the cloud collapse, that can arise due to the choice of three-body reaction rates. In what follows, we will first study the accretion rate as predicted by the properties of the gas in the clouds just before the first sink particle forms. We will then examine the accretion rate as measured by the sink particles themselves.

The accretion rate can be estimated from the radial gas profiles using,

$$\dot{M}(r) = 4\,\pi\,r^2\,\rho(r)\,v_{\rm rad}(r). \tag{2.1}$$

This has been shown to be a good estimate of the accretion rate (Clark et al., 2011a). In addition, one can define an accretion time from,

$$t_{\rm acc} = \frac{M_{\rm enc}(r)}{4\,\pi\,\rho\,v_{\rm rad}\,r^2}. \tag{2.2}$$

Since accretion is related to infall velocity, we also discuss the corresponding radial and rotational velocities. Figure 4.2 shows these physical quantities as the function of enclosed mass for all the simulations, using the radial profiles in the gas just before the formation of the first sink particle. The left panel of Fig. 4.2 in the clockwise order, shows the accretion rate, radial velocity, radial velocity over sound speed and accretion time respectively. Similarly the right panel of Fig. 4.2 shows the rotational velocity, radial velocity over rotational velocity, rotational velocity over Keplerian velocity and rotational velocity over sound speed respectively in the clockwise order.

We note that the mass accretion rate ($\dot{M}$) for all the simulations has a maximum at an enclosed mass $\sim$1–2 $M_\odot$. Given that H_2 line-cooling becomes optically thick at the corresponding densities for this enclosed mass, it makes sense that $\dot{M}$ for all simulations converge at this mass scale, as the gas loses its ability to cool efficiently. In general, the differences in accretion rates caused by the choice of three-body formation rate are small, around 25 percent. The differences between the rates in different halos are much larger, at around a factor of 2 for masses below a few tens of solar mass. However we see from the top left panel of Fig. 4.2 that once the mass approaches

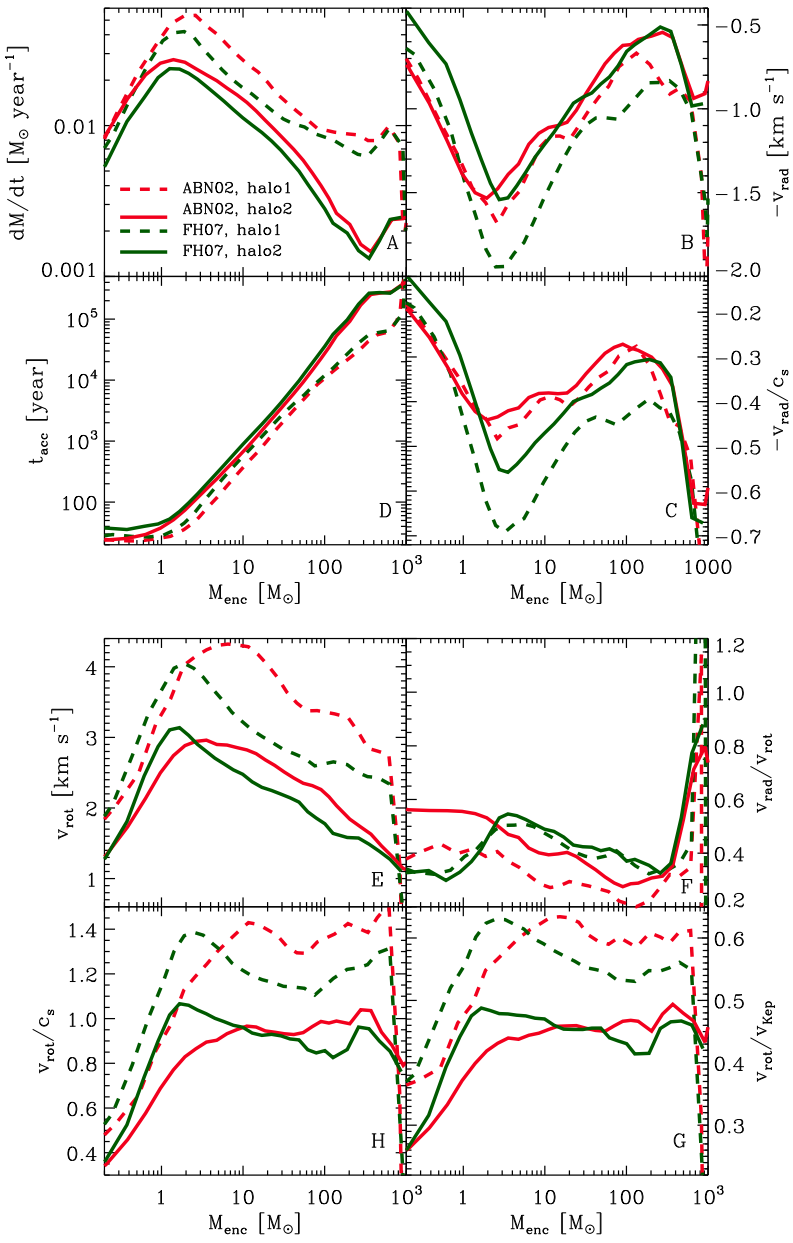

Figure 2.2: Radial logarithmic binned, mass-weighted averages of mass accretion rate (A), radial velocities (B), ratio of radial velocity to sound speed (C), accretion time (D), rotational velocity (E), ratio of radial to rotational velocity (F), ratio of rotational to Keplerian velocity (G) and ratio rotational velocity to sound speed (H) are plotted as a function of enclosed mass. The halo to halo variation as well as the uncertainty in the three-body rate introduce an uncertainty in the mass accretion rate, radial and rotational velocity.

$100\,M_\odot$, the difference in the accretion rates can be large, approaching an order of magnitude. We conclude that halo-to-halo variations will play a larger role in the accretion rates than chemical uncertainties.

The choice of three-body rate coefficient introduces difference in radial velocity of $\sim$0.4–0.5 km s^{-1}. We also note that the radial velocities for both rates are substantially lower than the rotational velocities. The gas particles spiral inwards with trajectories following a combination of gravitational attraction and angular momentum conservation. All clouds are sub-Keplerian. However, there is a slight tendency for the gas to be more rotationally supported in the FH07 runs – at least for the inner $10\,M_\odot$ of gas.

We can compare these results with both the AMR and SPH simulations of Turk et al. (2011). Our high-resolution study also concludes that the difference in the three-body H_2 formation rates significantly affect the dynamical behavior of the collapsing gas. The uncertainty in the velocity structure has also been investigated by Bovino, Schleicher & Grassi (2014) using hydrodynamics code ENZO. They also found that there are relatively large differences in the radial velocities of about 2–3 km s^{-1} depending on the halo distribution as well as three-body H_2 formation rates.

Although there is scatter in the velocities for ABN02 and FH07 rates, the scatter also exists in the velocities for both halo1 and halo2. We again conclude that the halo-to-halo differences in the velocity structure is, in general, more pronounced than that caused by the differences in the chemical reaction rates.

2.5 Fragmentation

We have shown in Section 3.3.1 that the temperature of the gas at high densities, such as those in disk, depends on the choice of adopted three-body H_2 formation rate. In this section, we study how the gas fragments as it evolves beyond the formation of the first collapsing core. Our discussion will first focus on the properties of the gas, to see whether there is any hint of the future evolution already present before the first sink particle forms. We will then compare the properties of the sink particles in the simulations and discuss the differences.

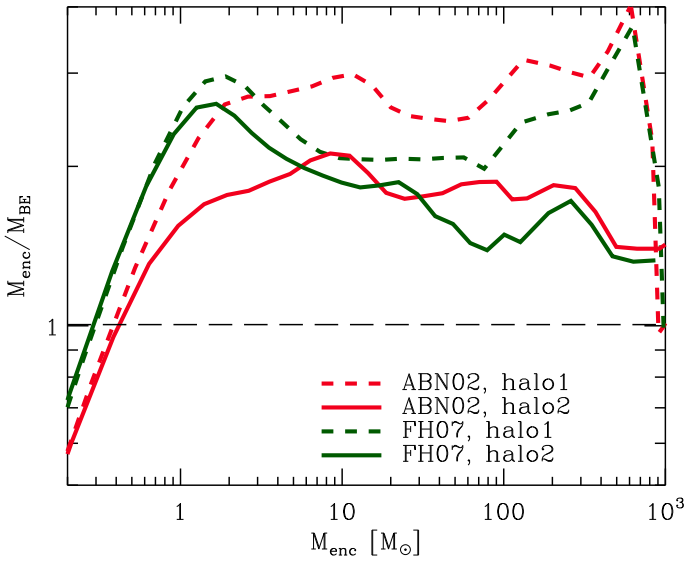

Figure 2.3: The number of Bonnor–Ebert masses ($M_{\rm enc}/M_{\rm BE}$) in the central dense volume is plotted as a function of enclosed mass, just before formation of first protostar. The degree of gravitational instability for FH07 within the central dense regime is larger than ABN02, indicating larger opportunity for the gas to fragment in the FH07 case, than in the ABN02 simulations.

One useful measure of the ability of the gas to fragment is the ratio of the thermal to gravitational energy. This can be represented by the number of Bonnor–Ebert masses ($M_{\rm BE}$) contained in the central dense volume (Ebert 1955; Bonnor 1956). We therefore investigate the changes in the number (i.e, $M_{\rm enc}/M_{\rm BE}$) for each of our simulations and how it varies with the enclosed gas mass, similar to the analysis performed by Abel, Bryan & Norman (2002). We computed the Bonnor–Ebert mass as the mass-weighted average within the logarithmic radial bin,

$$M_{\rm BE} = 1.18(c_s^4/G^{3/2})P_{\rm ext}^{-1/2} \approx 20 M_\odot T^{3/2} n^{-1/2} \mu^{-2} \gamma^2, \tag{2.3}$$

where c_s is the sound speed, $P_{\rm ext}$ is the external pressure that we assume to be equal to the local gas pressure, μ is the mean molecular weight and $\gamma = 5/3$ is the adiabatic index, respectively.

The results are shown in Fig. 4.3. Note that the ratio of the enclosed mass over Bonnor–Ebert mass (i.e., $M_{\rm enc}/M_{\rm BE}$), which measures the number of gravitationally unstable gas clumps, is equivalent to the ratio of fragmentation time-scale to that of accretion time-scale, $t_{\rm frag}/t_{\rm acc}$. Once again, these snapshots were taken immediately before the formation of the first protostar. The dashed lines represent the case when fragmentation time-scale equals the accretion time-scale.

While we see that there are differences between the mass profiles of the FH07 and ABN02 runs, the effects are, once again, not substantial. However, in the case of $M_{\rm enc}/M_{\rm BE}$ we see that the FH07 runs have a differently shaped profile from the ABN02 runs (top panel of Fig. 4.3). In the FH07 case, the profiles are peaked at characteristic mass of 1-2 $M_\odot$. In contrast, the ABN02 runs do not display such a peak, and it is less clear whether these runs would favour a particular mass for fragmentation.

If the ratio $M_{\rm enc}/M_{\rm BE} < 1$, the gas enclosed in the shells are accreted faster than it can fragment. As a result fewer new protostars are formed and the available mass contributes to the mass growth of the existing ones (Dopcke et al. 2013). In our case we find $M_{\rm enc}/M_{\rm BE} > 1$, i.e., the gas in the shells can fragment faster than it is accreted by the central dense clump, favouring low-mass protostars.

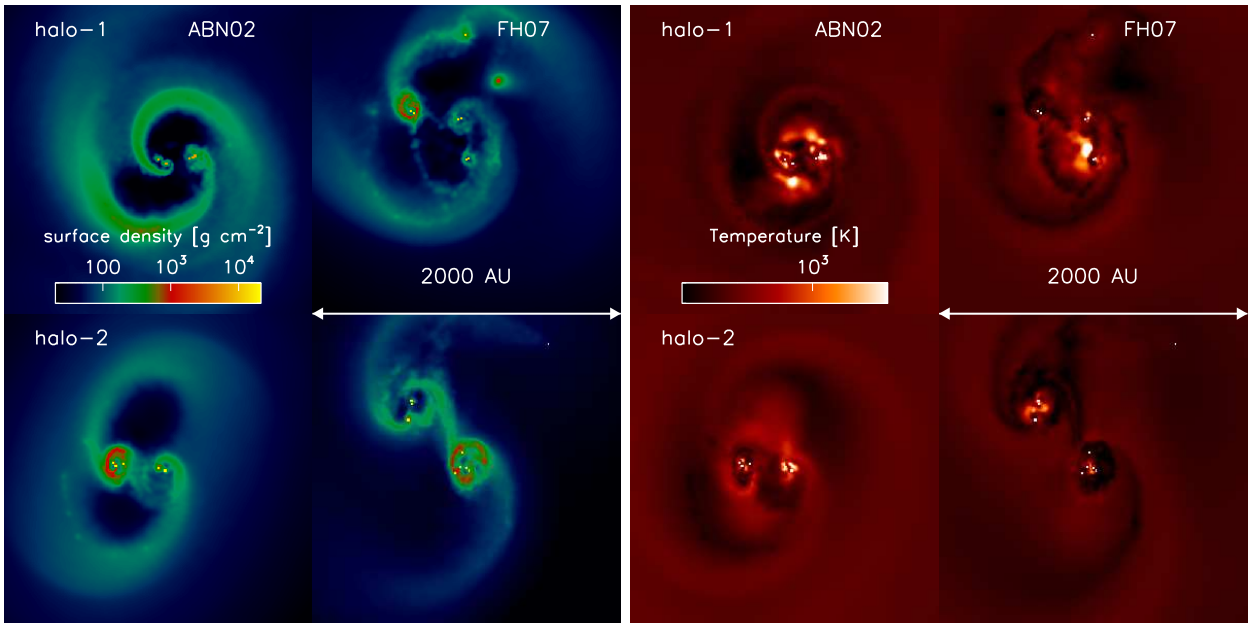

Figure 2.4: Surface density and temperature in a region of 2000 AU centred around first protostar for different three-body H_2 formation rates, are shown when the total mass of the sinks reaches $\sim 21\, M_\odot$.

Therefore by considering the radial density profiles before the onset of sink formation, we conclude that gas in FH07 case is perhaps more likely to fragment than in the ABN02 case. Next we study how the gas fragments at later epochs after formation of the first sink particle. We follow the simulations until 21 $M_\odot$ have been converted into, or accreted onto, sink particles.

We have calculated the total mass accretion rate by all the sinks particles. Although fragmentation may depend on the way sink particles are modelled, our implementation (Section 2.2.2) takes considerable care to avoid what is often called artificial fragmentation and the spurious formation of sink particles (further details are found in Clark et al. 2011, see also Bate, Bonnell & Price 1995, Jappsen et al. 2005, and Federrath et al. 2010).

The column density and column-weighted temperature distribution in the inner 2000 AU at the end of the simulations are shown in Fig. 4.4. In all cases we see that the simulations exhibit disk structure on several scales within this central region. It is not surprising, given the high levels of rotational support seen in right-hand panel in Fig. 4.2. We also see that the temperatures in the disk are slightly less in the case with the FH07 rate, due to the increased H_2 fraction. However from these images it is clear that all simulations fragment to form a small-N system within the time that 21 $M_\odot$ of material is accreted onto sink particles.

Figure 2.5A shows the time evolution of total mass accretion rate onto the sinks (same as Fig. 4.2). The plot shows that mass accretion rate for ABN02 is larger than the FH07 rate. For both rates, $\mathrm{d}M^*/\mathrm{d}t$ decreases with time. After ≈500 years, further sink particles form, and the total accretion rate increases again, however, now with large temporal variations. In Fig. 2.5B, we plot the mass accretion rate as a function of total sink mass. Figure 2.5C shows the time evolution of the total mass in sinks and Figure 2.5D shows the maximum sink mass in the period over which the sink formation occurs.

We see that the simulations employing the ABN02 rate produce a maximum sink mass that is consistently above the FH07 rate, for a given halo. However, the difference is less than a factor of 2 and is similar to the interhalo difference. When we examine the Figure. 2.5E, which shows the total number of sink particle versus the total mass

in all sinks, we see a similar behavior; the differences between the runs with different rates can be a factor of two. Although in this case the halo-to-halo differences are less pronounced.

We caution the reader that our simulations do not include feedback effects from nascent protostars. We therefore restrain ourselves from following the dynamical evolution of the embedded stellar system over very long time-scales. We end our calculations before we expect that radiative and mechanical feedback changes the thermal as well as chemical state – and as a consequence – also modifies the fragmentation behavior of the remaining gas (see, e.g., the discussion in Wise & Abel 2008, Whalen, Hueckstaedt & McConkie 2010, Hosokawa et al. 2011, or Stacy et al. 2012).

2.6 Summary

We have investigated the effects of different proposed three-body H_2 formation rates during the collapse of primordial star-forming clouds and analysed their influence on the resulting fragmentation behavior of the gas. We compared the rates proposed by Abel, Bryan & Norman (2002) and by Flower & Harris (2007), which span two orders of magnitude. We follow the chemical and thermal evolution of the primordial gas in two different minihalos in order to assess differences introduced by varying halo parameters. We find that the uncertainty in the three-body H_2 formation rates leads to the differences in the chemical state of the gas which is more important for the thermal evolution of the clouds than any differences in the halo properties. The halo to halo variation affects the dynamical evolution of the gas and mass-accretion more than the chemical uncertainties.

We also find that the simulations employing the Abel, Bryan & Norman (2002) rate to produce on average fewer and more massive fragments compared to those calculations using the Flower & Harris (2007) rate (consistent with the results of Bovino, Schleicher & Grassi (2014) which however did not use sink particles). This difference of roughly a factor of 2, however, is comparable to the halo-to-halo variation. This is similar to the results reported by Turk et al. (2011) with added advantage of using sink particles.

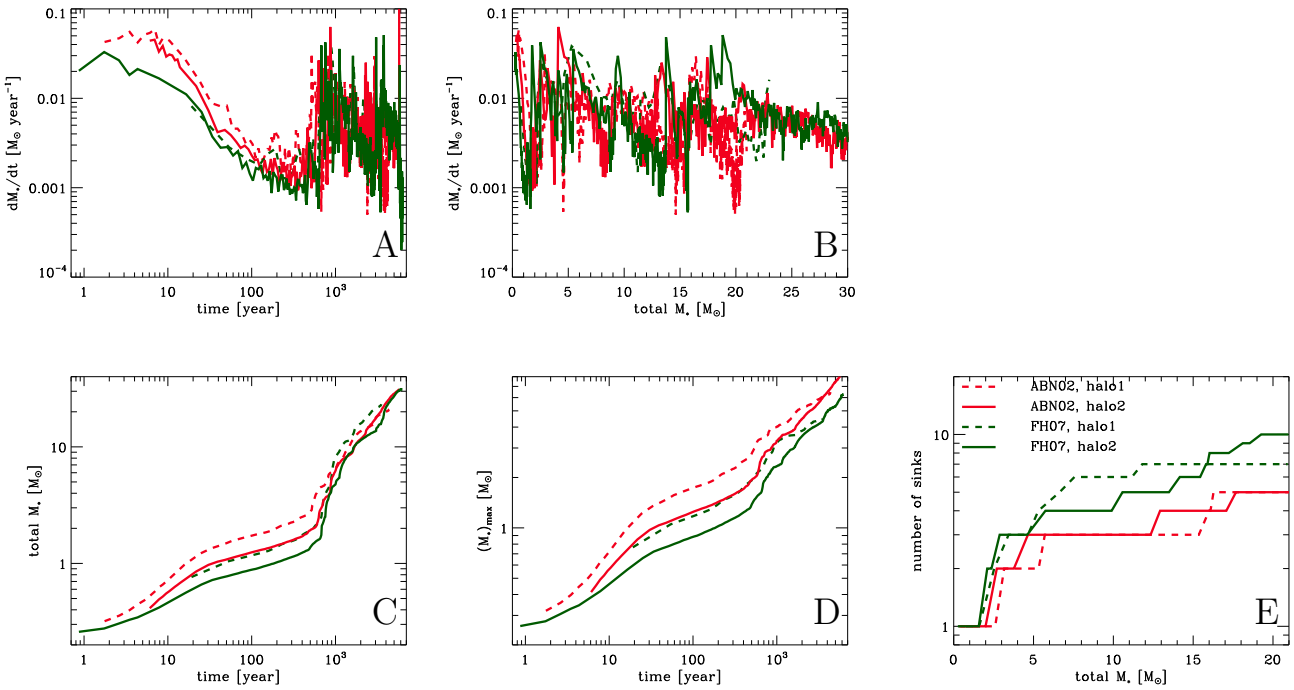

Figure 2.5: Time evolution of the protostellar system: accretion rate as the function of time (A) and total mass in sink particles (B). The total mass of all the sinks particles (C) and the most massive sink particle (D) are plotted as function of time. The simulations employing FH07 produce more fragmentation than ABN02 (E).

In summary, we find that the variations introduced to the mass distribution of primordial stars as a result of the uncertainties in the three-body H_2 formation rate is of similar order to the fluctuations in the halo properties.

Chapter 3

Does the chemothermal instability have any role in the fragmentation of primordial gas

The collapse of the primordial gas in the higher density regime $\sim 10^8$–10^{10} cm^{-3} is controlled by the three-body H_2 formation process, in which the gas can cool faster than free-fall time—a condition proposed as the chemothermal instability. We investigate how the heating and cooling rates are affected during the rapid transformation of atomic to molecular hydrogen. With a detailed study of the heating and cooling balance in a 3D simulation of Pop III collapse, we follow the chemical and thermal evolution of the primordial gas in two dark matter minihalos. The inclusion of sink particles in modified GADGET-2 smoothed particle hydrodynamics code allows us to investigate the long-term evolution of the disk that fragments into several clumps. We find that the sum of all the cooling rates is less than the total heating rate after including the contribution from the compressional heating (pdV). The increasing cooling rate during the rapid increase of the molecular fraction is offset by the unavoidable heating due to gas contraction. We conclude that the H_2 cooling, the heating due to H_2 formation and compressional heating together set a density and temperature evolution in the disk that favors fragmentation, not the chemothermal instability.

3.1 Introduction

Understanding the first source of light in the Universe, the so-called primordial stars or Population III (Pop III) stars, is crucial in determining how the Universe evolved into what we observe today (Bromm & Yoshida 2011; Bromm 2013; Glover 2013). With the help of state-of-the-art simulations along with the well established cosmological parameter (Planck Collaboration et al. 2014), recent studies have provided a standard model of the Pop III star formation (e.g., Greif et al. 2012; Johnson, Dalla & Khochfar 2013; Stacy et al. 2013; Hirano et al. 2014, 2015; Hartwig et al. 2015). In this picture, the baryons (mainly atomic hydrogen) in low mass ($\sim 10^5$–10^6 $M_\odot$) dark matter halo with virial temperature $\sim$1000 K gravitationally collapsed at redshift $z \geq 20$ via H_2 molecular cooling to form the very first stars in the Universe (Haiman et al. 1996; Tegmark et al. 1997; Barkana & Loeb 2001; Ciardi & Ferrara 2005).

Initially the gas is cooled via H_2 rotational and vibrational line emission (Susa et al. 1998; Omukai & Nishi 1998). However, the quick conversion of atomic hydrogen into molecules via the three-body reactions: 1.4,1.5 can cool the gas rapidly at high densities ($\sim 10^8$ cm^{-3}). This results in the gas to be chemothermally unstable (Yoshida et al. 2006; Turk, Abel & O'Shea 2009). The physical processes are extremely complex during the three-body reaction. The gas undergoes both heating and cooling simultaneously. Heating is due to the release of 4.4 eV energy associated with every H_2 formation and gas contraction, and cooling is due to the emission, dissociation of H_2 and collisions of H_2. However, there is little understanding of the interplay between the heating and cooling rates so far.

In addition, the physics at high densities is relevant to the inception of the thermal instability (first predicted by e.g., Sabano & Yoshii 1977; Silk 1983) that can generate fluctuations in the gas density in a comparatively shorter interval than the collapse time. The numerical simulations by Abel, Bryan & Norman (2002) found several chemothermally unstable regions. They have, however, pointed out that the instabilities do not lead to fragmentation as the turbulence efficiently mixes the gas, thereby erasing the fluctuations before they can grow significantly. In a different approach, Omukai & Yoshii (2003) have calculated the stability of the gas cloud for

isobaric perturbations by introducing the 'growth parameter (Q)', which must be significantly larger than unity for a clump of gas to break into multiple objects. A detailed analytical calculation of the instability criterion has been investigated by Ripamonti & Abel (2004). The high resolution 3D ΛCDM cosmological simulation by Yoshida et al. (2006) has shown that the growth parameter indeed never becomes much larger than unity. It is infact less than 1.5, which implies that the chemothermal instability cannot lead to any fragmentation. A similar conclusion was drawn by Turk, Abel & O'Shea (2009). In contrast, more recently Greif, Springel & Bromm (2013) have used AREPO simulations to follow the evolution of the gas in minihalos that fragments. They have suggested that this is due to the chemothermal instability because the ratio of the cooling time-scale to the free-fall time-scale drops below unity in the density space where the three-body reaction dominates.

Our approach to study the chemothermal instability as the sole reason for fragmentation scenarios is significantly different from those in the previous works. For example, for the first time to the best of our knowledge, we investigate the heating and cooling balance in a full 3D simulation of Pop III collapse to understand better the physical processes during the rapid conversion of atomic to molecular hydrogen. The closest study so far would be the analysis by Omukai et al. (2005). However, they examined idealized 1D collapse models without exploring the uncertainties in the three-body rates. In this paper, we investigate the chemothermal instability by comparing different heating and cooling rates and discuss their roles in the fragmentation during the long-term evolution of the disk.

3.2 Numerical Methodology

The simulation setup and initial conditions are similar to our previous study (Dutta, Nath, Clark & Klessen 2015) that used minihalos from the cosmological simulations of Greif et al. (2011). Both the halos start with a maximum central cloud number density $n \sim 10^6$ cm^{-3}, the density before the onset of the three-body reaction. The details of the halo properties are given in Table 3.1. We use the halo configurations as the initial condition for our standard smoothed particle hydrodynamics (SPH) code GADGET-2

Table 3.1: Summary of minihalos from the cosmological simulations.

Halo properties	halo1	halo2
n (cm^{-3})	10^6 (max) 71 (min)	10^6 (max) 85 (min)
T (K)	469 (max) 59 (min)	436 (max) 54 (min)
Mass ($M_\odot$)	1030	1093
n-SPH	690855	628773
resolution ($M_\odot$) for 100 n-SPH	1.3 $\times 10^{-2}$	1.4 $\times 10^{-2}$

Note: n-SPH stands for the number of SPH particles in the simulation.

(Springel 2005) that has been modified with the inclusion of sink particles (Bate, Bonnell & Price 1995; Jappsen et al. 2005) and time-dependent chemical network for primordial gas (Clark et al. 2011a). The snapshots from the hydrodynamic moving mesh code AREPO (Springel 2010) are converted into the GADGET-2 implementation (Smith et al. 2011). This is possible because the mesh-generating points of AREPO can be interpreted as the Lagrangian fluid particles. The mass resolution in our GADGET-2 simulation is $\approx 10^{-2}$ $M_\odot$ for 100 SPH particles (Bate & Burkert 1997).

Once the gas density reaches $\sim 10^{10}$ cm^{-3}, the cloud becomes opaque and the strongest of H_2 lines becomes optically thick. The H_2 cooling rate in this regime is calculated using the Sobolev approximation (as described in Yoshida et al. 2006). At densities $\geq 10^{14}$ cm^{-3}, the gas goes through a phase of cooling instability due to rapid increase in the cooling rate by H_2 collisional induced emission (CIE). We follow Ripamonti & Abel (2004) to use the rate in our cooling function. Above the central density $\sim 10^{16}$ cm^{-3}, the gas becomes completely optically thick to the continuum radiation (Yoshida, Omukai & Hernquist 2008). At this point, the remaining H_2 dissociates by collisions with the atomic H and other H_2 molecules, and consequently cools the gas resulting in further collapse.

We ensure that our investigation is not biased on the chemical uncertainties and halo configuration. Hence, we simulate the gas evolution in two different minihalos with the extreme three-body rate coefficients: Abel, Bryan & Norman (2002) (hereafter ABN02) provide the slowest rate, Flower & Harris (2007) (hereafter FH07)

provide the fastest rate. Using the highly simplified one-zone models, the works by Glover & Abel (2008) and Glover & Savin (2009) examined minutely the effects of the uncertainty in the three-body H_2 formation rates and the cooling rate on the thermal evolution of the collapsing gas in simple Bonnor-Ebert spheres (Ebert 1955; Bonnor 1956). They have found that the large uncertainty between the ABN02 and FH07, which differ by a large amount, lead to an uncertainty of approximately 50% in the temperature evolution of the gas in the density range $10^8 < n < 10^{13}$ cm^{-3}.

The primordial protostar can be modeled as a sink particle (Krumholz, McKee & Klein 2004), which basically replaces the high-density region as a protostar that can accrete infalling mass. In our simulations, the protostar is formed once the number density of the gas reaches 5 $\times 10^{13}$ cm^{-3} and temperature is $\sim$1000 K. The Jeans mass at this critical point is $M_{\rm J}$ (1000 K, 10^{13} cm^{-3}) $\sim 0.06\ M_{\odot}$ and Jeans radius is 6 AU, which is the accretion radius, $r_{\rm acc}$, of the sink particle. The spurious formation of new sink particles is avoided by preventing the sink particles from forming within $2\,r_{\rm acc}$ of one another. Depending on the halo configurations and chemical uncertainties, our simulations run $\approx$3500–6500 year after the formation of the first protostar.

3.3 Results

3.3.1 Chemothermal instability

As the gas undergoes gravitational collapse, the crucial aspect to be investigated is whether the gas will be able to cool significantly or not. The rapid formation of hydrogen molecules via three-body reactions allows the gas to cool in less than a free-fall time, heralding chemothermal instability. This effect for both the ABN02 and FH07 rates has been shown by Dutta, Nath, Clark & Klessen (2015), where we have found that the ratio of the cooling time to the free-fall time ($t_{\rm cool}/t_{\rm ff}$) dips below unity at a certain density. This is exactly what Greif, Springel & Bromm (2013) have found in their simulations. In our present calculation, we have considered all the cooling mechanisms, including the contributions from chemical heating, to calculate the cooling time: $t_{\rm cool} = \epsilon/\Lambda_{\rm net}$, where ϵ is the energy per unit volume of the gas

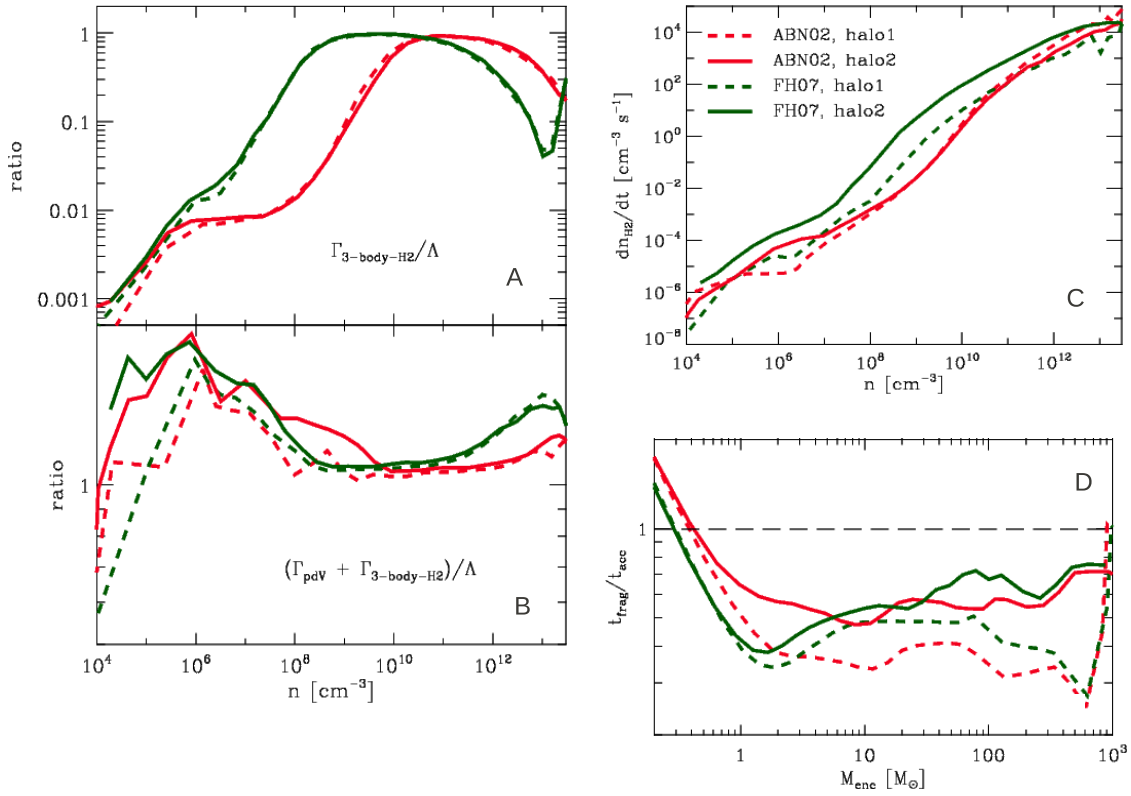

Figure 3.1: Radially binned, mass-weighted averages of the physical quantities for different proposed three-body H_2 formation rates (red: ABN02, green: FH07) of two cosmological halos (dotted: halo1, solid: halo2) are compared just before the first protostar is formed. (A) The ratio of the three-body formation heating to the total cooing rate, (B) ratio of the total heating to the total cooling rate and (C) the rate of H_2 formation (dn_{H_2}/dt) from the simulations in the units of cm^{-3} s^{-1} are plotted as a function of density. (D) The fragmentation time over the accretion time is plotted as a function of enclosed gas mass.

and $\Lambda_{\rm net}$ is the net cooling rate in units of erg s^{-1} cm^{-3}. This implies that the gas can cool as it collapses, and is hence undergoing chemothermal instability. It is to be noted that the drop in the ratio $t_{\rm cool}/t_{\rm ff}$ coincides with the onset (in density space) of the three-body H_2 formation (Greif, Springel & Bromm 2013; Dutta, Nath, Clark & Klessen 2015).

However, as we have discussed in Section 5.1, there is still some discrepancy of whether the fragmentation is stimulated by the chemothermal instability or not. Fragmentation might also depend on other details, such as turbulence, rotation, etc (see for examples, Turk, Abel & O'Shea 2009; Stacy, Greif & Bromm 2010; Clark et al. 2011; Latif et al. 2015; Dutta 2015). The variation of the ratio of the cooling time to the free-fall time in the density space, where the three-body reactions take place, is too simple to make a definite conclusion about the fragmentation. A straightforward analysis involves comparing all possible heating and cooling processes that are responsible for setting the thermal balance in the gas.

3.3.2 Heating and Cooling rates

In this section, we investigate the relevant cooling and heating mechanisms associated with the emission, chemical reaction and gas contraction during collapse. The synchronous effects of the cooling and heating rates make the chemical and thermodynamical evolution complicated

Assuming the evolution of the gas density (ρ) with the free-fall time ($t_{\rm ff}$), i.e., $\mathrm{d}\rho/\mathrm{d}t = \rho/t_{\rm ff}$, previous studies (e.g., Omukai 2000; Bromm, Coppi & Larson 2002) show that the thermal evolution is followed by solving the energy equation:

$$\frac{\mathrm{d}\epsilon}{\mathrm{d}t} = \frac{p}{\rho}\frac{\mathrm{d}\rho}{\mathrm{d}t} - \Lambda + \Gamma, \tag{3.1}$$

where Λ and Γ are the cooling and heating rate respectively in units of erg s^{-1}cm^{-3}. This can be seen in Figure 3.1 in which we compare the various heating and cooling rates in the simulation as a function of density. All the quantities are mass-weighted averages of the individual SPH particles that are binned logarithmically in radius. These logarithmic-binned spherical shells are centered at the origin at $r = 0$.

We have rigorously verified that the mass-weighted averaging does not throw away any physical information. The calculations are done once the central region has collapsed to a density $\sim 5 \times 10^{13}$ cm^{-3}, i.e., just before the formation of the first sink.

We take the total cooling rate as the sum of the H_2 line-cooling rate, collision induced emission cooling rate (CIE) and dissociation rate (i.e., $\Lambda = \Lambda_{\rm line} + \Lambda_{\rm CIE} + \Lambda_{\rm Diss}$) and total heating rate as the combination of heating from the compression (pdV) and the three-body formation of H_2 (i.e., $\Gamma = \Gamma_{\rm pdV} + \Gamma_{\rm 3-body-H2}$).

Figure 3.1A shows that the total cooling can be as high as the heating associated with the three-body formation of H_2, and thus the ratio of $\Gamma_{\rm 3-body-H2}$ to Λ is of order unity in the density space where the three-body reaction dominates. The three-body heating rates for the FH07 rise before the ABN02 do because the higher H_2 formation rates of FH07 cause the gas to become fully molecular at lower densities. As a result, the gas in the FH07 case becomes optically thick at earlier times, preventing the thermal energy from being transported efficiently out of the disk. We have verified that other cooling processes, such as the heat loss due to the collisional dissociation or the collision induced emission are not effective until much higher densities.

Most importantly, when including the contribution from compressional heating, we notice that the total heating rate is always greater than the total cooling rate of the gas (Figure 3.1B). For the gas to be chemothermally unstable to fragmentation, the heating and cooling rate must satisfy the condition:

$$\Lambda_{\rm line} + \Lambda_{\rm CIE} + \Lambda_{\rm Diss} \geq \Gamma_{\rm pdV} + \Gamma_{\rm 3-body-H2}\,, \tag{3.2}$$

that could occur due to a sharp increase in the fractional abundances. However, in our case, the total heating rate dominates even in the high density regime. This leads to an ever increasing temperature with density.

From this analysis, we tentatively conclude that the gas can experience a dip in the ratio of the cooling time to the free-fall time in the density space, and hence becomes chemothermally unstable. However, the rapid cooling due to the three-body reaction is countervailed by the compressional heating. Thus it never leads to significant drop in the temperature. This is consistent with the previous studies (e.g., Abel, Bryan &

Norman 2002; Bromm, Coppi & Larson 2002; Ripamonti & Abel 2004; Yoshida et al. 2006).

At this point, we would like to point out the differences with the work by Greif, Springel & Bromm (2013). The use of the ratio $t_{\rm cool}/t_{\rm ff}$ as a criterion for fragmentation and collapse by Greif, Springel & Bromm (2013) neglects the heating due to the formation of H_2 and pdV contraction. This heating generally exceeds H_2 cooling and dominates the temperature and density evolution of the collapsing gas, and hence its tendency to fragment and form new stars.

Another point to note is that a change in the analysis of the ratio, $t_{\rm cool}/t_{\rm ff}$, does not necessarily coincide with a change in the ratio of the free-fall time to the sound crossing time–which is a measure of the number of Jeans masses. Note that Turk, Abel & O'Shea (2009) were the first to find the fragmentation in the Pop III star forming halos because they included the heating due to H_2 formation, whereas Yoshida, Omukai & Hernquist (2008) did not. These studies along with our detailed rigorous analysis support the claims that the contribution from both the three-body H_2 formation heating and compressional heating must be included to capture the fragmentation in the Pop III star forming halos.

3.3.3 The formation rate of H_2

Since the onset of the chemothermal instability is strongly associated with the formation of hydrogen molecules, it is therefore instructive to examine the rate at which H_2 actually forms in the collapse calculations.

We calculate the H_2 formation rate ($dn_{\rm H_2}/dt$) from the data generated in our simulations and plot as a function of density in Figure 3.1C. To create these plots, we first calculate the number density of hydrogen molecules on a mass shell that has a particular density and temperature for a specific epoch (i.e., for a given snapshot at time t_1). For the same snapshot, we then keep on calculating the number density of hydrogen molecules for different mass shell (each of which has a particular density and temperature). Both the density and temperature are radially-logarithmic binned, mass-weighted averages. We repeat the procedure for the consecutive snapshot of time

t_2. We compare the H_2 abundances in these snapshots from the simulations over a time interval $\Delta t = t_2 - t_1$, with the rates given by

$$\frac{\mathrm{d}n_{\mathrm{H_2}}}{\mathrm{d}t} = \frac{n_{\mathrm{H}}(t_2)y_{\mathrm{H_2}}(t_2) - n_{\mathrm{H}}(t_1)y_{\mathrm{H_2}}(t_1)}{t_2 - t_1}. \tag{3.3}$$

Note that an assumption here is made that the number density of the gas between the two snapshots does not change significantly and the time interval Δt is chosen as small as possible (≈8 months, considerably small compared to both the free-fall and cooling times).

Over the range of densities in which the three-body reactions are important (i.e., above 10^7 cm^{-3}), we find that the differences in $\mathrm{d}n_{\mathrm{H_2}}/\mathrm{d}t$ between the simulations are strongly density dependent. Around a density of $\sim 10^8$–10^9 cm^{-3}, the difference between the formation rates in the simulations is the highest. The curve is steeper in this regime, allowing us to infer that the rapid production of hydrogen molecules can cool the gas promptly and hence trigger the cooling time to be shorter than the free-fall time.

Note that at high densities this method is no longer strictly applicable as it is highly sensitive to the chosen time interval. However, this calculation provides a good estimate for the overall trend of the rate of H_2 formation inside the halos in which we are particularly interested.

3.3.4 Fragmentation and long term evolution

Fragmentation can be manifested in various terms, as it depends on the thermal and chemical history, interaction with the surroundings, gas mass and instability in the clouds. Here we focus on how the thermo-dynamical evolution due to the heating and cooling rates can provide a hint of future fragmentation in our calculations.

One can measure the instability in the gas by computing the number of Jeans mass, or more appropriately the Bonnor-Ebert mass (M_{BE}) inside the central dense volume (Ebert 1955; Bonnor 1956). This is same as comparing the fragmentation time-scale (t_{frag}) with the accretion time-scale (t_{acc}). In other words, the ratio, $t_{\mathrm{frag}}/t_{\mathrm{acc}}$, is equivalent to the ratio, M_{BE}/M, i.e., the inverse of the number of Bonnor-Ebert mass

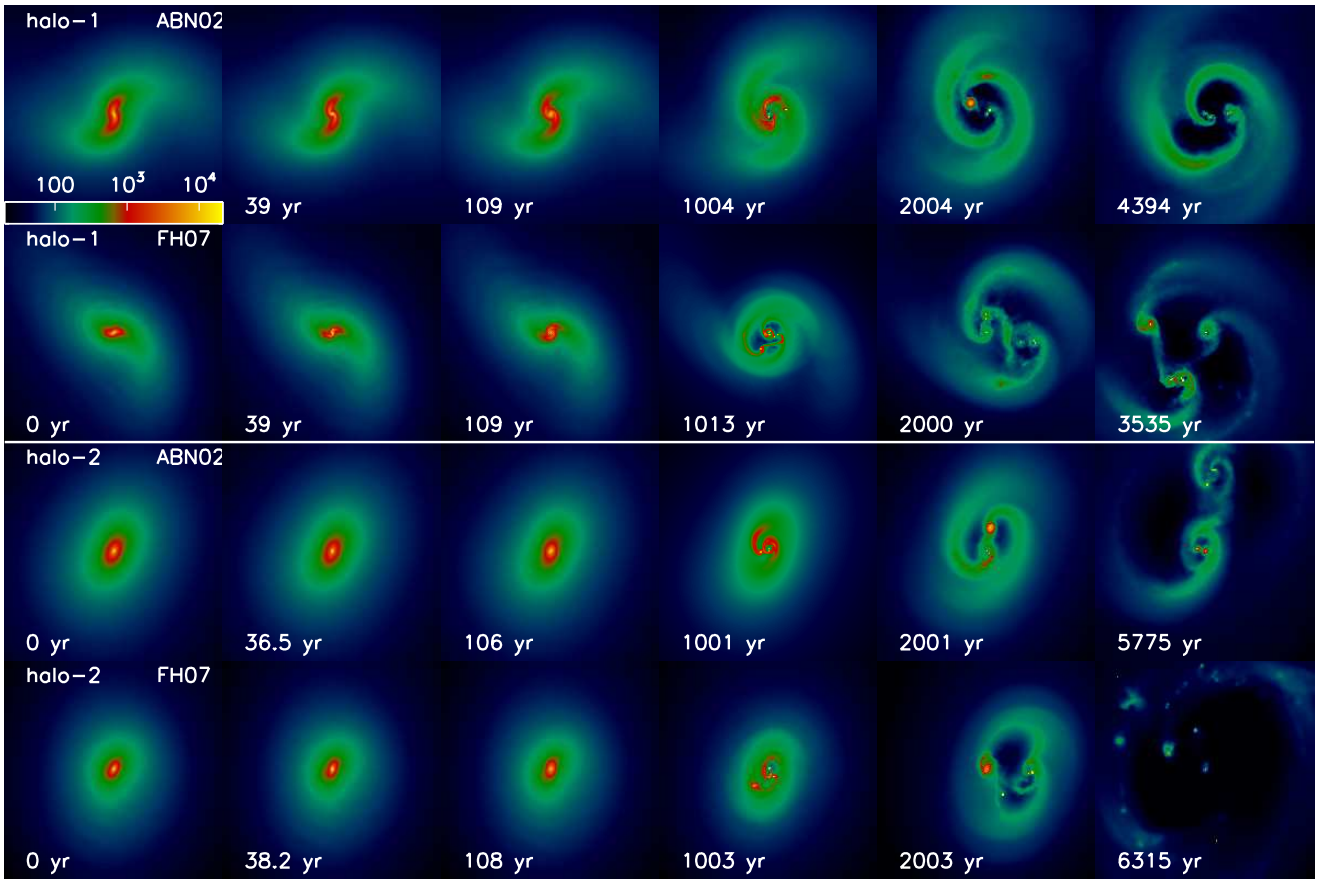

Figure 3.2: Evolution of surface density in the disk at later epochs in a region of 2000 AU centred around first protostar in the cosmological minihalos for different proposed three-body H_2 formation rates.

masses enclosed in the central volume. We define the fragmentation time-scale as the rate of change in the number $M_{\rm BE}$ within a given radial shell (Dopcke et al. 2013),

$$t_{\rm frag} \equiv \frac{M_{\rm BE}}{\dot{M}}, \tag{3.4}$$

and compare it with the accretion time-scale $t_{\rm acc}$ (Abel, Bryan & Norman 2002). The results are shown in Figure 3.1D. The snapshots were taken just before the formation of the first protostar. The dashed lines represent the case when fragmentation time-scale is equal to the accretion time-scale.

If $t_{\rm frag}/t_{\rm acc} > 1$, the gas enclosed in the shells is accreted faster than it can fragment. As a result, fewer new protostars are formed and the available mass contributes to the mass growth of the existing ones. In our case, we find $t_{\rm frag}/t_{\rm acc} < 1$, i.e., the gas in the shells can fragment faster than it is accreted by the central dense clump, favouring low-mass protostars. Therefore, comparing only the time-scale, we get an indication of the possible fragmentation from the thermo-dynamical evolution of the gas before the onset of the sink formation.

At later epochs, we follow the simulations for ≈3500–6500 year (depending on the cosmic variance of the minihalos) after the formation of the first sink particle. The column density in the inner 2000 AU at the end of the simulations are shown in Figure 4.4. In all cases we see that the simulations exhibit the disk structure that fragments on several scales within this central region. We can also see that the density in the disk are slightly less in the case with the FH07 rate due to the increased H_2 fraction. The disk evolves with time with the matter accreted on to sink particles, and becomes more and more Jeans unstable.

We conclude that the temperature continues to rise with increasing density meaning that there is no preferred scale at which fragmentation takes place during the collapse. Any future fragmentation is likely to be a result of the drop in the Jeans mass that is a strong function of temperature. Hence the intricate combination of the heating and cooling rates during the three-body reaction plays a significant role in determining the unstable clumps in the cloud.

3.4 Summary

We have investigated the diverse cooling and heating mechanism in two cosmological minihalos during the gas collapse to higher density. We have compared the physical processes with the extreme three-body rates proposed by ABN02 and FH07.

We argue that although the quantity $t_{\rm cool}/t_{\rm ff}$ might determine the onset of the chemothermal instability, the increase in the H_2 cooling throughout the fully molecular gas is offset by H_2 formation heating with compressional heating. Hence the thermal instability need not necessarily be the criterion for possible fragmentation. Rather, the thermo-dynamical evolution that depends largely on the complicated combination of the heating and cooling rates develops the unstable clumps by affecting its Jeans mass. This leads the disk to fragment on a scale of 1000-2000 AU. However, the scale in which the fragmentation takes place depends on the three-body H_2 formation rates. For example, simulations employing the ABN02 rate produce on average fewer and more massive fragments near the center, compared to those calculations using the FH07 rate (Dutta, Nath, Clark & Klessen 2015). However, the scale of fragmentation is comparable to the halo-to-halo variation. Our conclusion agrees well with the study by Ripamonti & Abel (2004) and Yoshida et al. (2006) that pointed that although the three-body reaction results in chemothermal instability, the growth of fluctuations are too small to lead to any fragmentation. Despite considerable computational efforts involved, we emphasize here that we cannot rule out the plausible concept of the chemothermal instability as the sole reason in all Pop III disk fragmentation scenarios. This is because of the fact that we have only considered two realizations. It is therefore of immediate interest to investigate the chemothermal instability in a number of minihalos, like those in Hirano et al. (2014).

In summary, we have explicitly shown various heating and cooling rates in a 3D simulation of Pop III collapse. This unique approach to the problem enables us to conclude that the fragmentation behavior does not necessarily happen due to the chemothermal instability. Instead, fragmentation occurs when H_2 cooling, the heat released by H_2 formation, and pdV compressional heating together set the Jeans mass in the gas to values that are conducive to breakup and collapse.

Chapter 4

On the effects of rotation in primordial star-forming clouds

The thermodynamical evolution of gas during the collapse of the primordial star-forming cloud depends significantly on the initial degree of rotation, which may originate from the non-axisymmetric nature of the cloud or slightly perturbed structure. However, there is little understanding of how the cloud's initial rotation affects the heating, cooling process and hence the temperature. We report the results from three-dimensional SPH simulations of a rotating self-gravitating primordial cloud with a modified GADGET-2 code, in which the initial ratio of the rotational to the gravitational energy (β_0) is varied over two orders of magnitude. We find that despite the lack of any initial turbulence and magnetic fields in the clouds, the angular momentum distribution leads to the formation and build-up of a disk that fragments into several clumps. We further examine the behavior of the protostars that form in both idealized as well as more realistic minihalos from the cosmological simulations. The thermodynamical evolution and the fragmentation behavior of the cosmological minihalos are similar to that of the artificial cases, especially in those with a similar β_0. Protostars with a higher rotation support exhibit spiral-arm-like structures on several scales, and have lower accretion rates. These type of clouds tend to fragment more, while some of the protostars escape from the cluster with the possibility of surviving until the present day. They also take much longer to form compared to their slowly rotating

counterparts. We conclude that the use of appropriate initial conditions of the gas in minihalos is a pivotal and decisive quantity to study the evolution and final fate of the primordial stars.

4.1 Introduction

Since the late 1960s, the theoretical study of the universe at high redshift has persuaded a number of groups to work persistently on the dynamics of collapsing gas clouds (Saslaw & Zipoy 1967; Peebles & Dicke 1968; Silk 1977; Couchman & Rees 1986), leading to the formation of the very first stars in the universe, the so-called Population III (or Pop III) stars. Based on these leading-edge studies, the first sources of light are believed to have formed only a few hundred million years after the Big Bang (Barkana & Loeb 2001; Bromm & Larson 2004; Ciardi & Ferrara 2005). This era marks a crucial transition from the simple to the complex universe (Loeb 2010; Bromm & Yoshida 2011; Glover 2013). Subsequent pioneering three-dimensional numerical simulations using adaptive mesh refinement (Abel, Bryan & Norman 2000; O'Shea & Norman 2006), smoothed-particle hydrodynamics (Yoshida, Omukai & Hernquist 2008) or more recently using the hydrodynamic moving mesh code AREPO (Greif et al. 2011, 2012) have led to the development of a widely accepted standard model of primordial star formation. In this star formation model, the first protostars form within dark matter (DM) halos with a virial temperature of $\sim$1000 K and masses of $\sim 10^5$–$10^6\ M_\odot$, which had collapsed at redshift $z \geq 20$. However, other simulations show that Pop III stars may still form well beyond this, in waves that delay their formation (e.g., Scannapieco, Schneider & Ferrara 2003; Tornatore, Ferrara & Schneider 2007; Ritter et al. 2012). These studies suggest that Pop III star can continue to form down to the redshift $z = 2.5$ with a low peak rate of $10^{-5}\ M_\odot\ \mathrm{yr}^{-1}\ \mathrm{Mpc}^{-3}$, which occurred at $z = 6$. Observational evidence of Pop III stars and the possibility of Pop III waves reaching lower redshifts has received a significant boost with the discovery of a luminous Lyman-α (Lyα) emitter with high EW He II and Lyα emission and no metal lines (Sobral et al. 2015).

Earlier studies show that the hydrogen atoms fall into the potential well of the dark

matter halos and are shock heated to a temperature that is close to the virial temperature of the halo (Haiman et al. 1996; Tegmark et al. 1997; Bromm, Coppi & Larson 1999). The hydrogen atoms then combine with the free electron to produce small fractional abundance of molecular hydrogen (McDowell 1961), which cools the gas through the rotational and vibrational line emission (Omukai & Nishi 1998; Susa et al. 1998). As the collapse proceeds to higher densities, hydrogen molecules are formed by the three-body formation reactions 1.5,1.6 (Palla, Salpeter & Stahler 1983). The rapid formation of hydrogen molecules at higher densities can promote the chemothermal instability in the gas (see, e.g.,Omukai & Yoshii 2003; Yoshida et al. 2006; Turk, Abel & O'Shea 2009; Dutta 2015). However, the rate coefficients for the three-body H_2 reactions span over two order of magnitudes (Glover & Savin 2009). Continued collapse leads to the gas becoming optically thick to the strongest of H_2 lines (Ripamonti & Abel 2004; Glover 2005). Above the central density $\sim 10^{16}$ cm^{-3}, the gas becomes completely optically thick to the continuum radiation (Yoshida, Omukai & Hernquist 2008).

The vanguard numerical simulations (see, e.g., Abel, Bryan & Norman 2002; Bromm & Larson 2004; Yoshida et al. 2006; O'Shea & Norman 2007; Wise & Abel 2008; Bromm, Yoshida, Hernquist & McKee 2009) propose the formation of massive (typically $\sim$20–50$M_\odot$) primordial protostars. This calculation result, however, contrasts with the present day star formation in which protostars with masses less than 1 $M_\odot$ are formed (Kroupa 2002; Chabrier 2003). The recent improved and high resolution numerical simulations have inferred that the disk around the primordial core is unstable and fragments to form a small N system with low-mass stars, instead of a single protostar (e.g., Stacy, Greif & Bromm 2010; Clark et al. 2011; Hirano et al. 2014; Hartwig et al. 2015).

In the literature, there are appreciable indications that the collapsing cloud from which the protostar forms could have strong rotational support (Larson 1969, 1984). The cloud's rotation can affect the dynamical as well as the thermal evolution of gas and consequently determine the ensuing properties of the Pop III stars (Bodenheimer 1995; Matsumoto, Hanawa & Nakamura 1997). The consequences of the cloud's rotation on the chemical signature of the zero-metallicity primordial stars have been

studied using stellar models (Meynet 2009, and references therein). With the use of the sink particle technique (discussed in §5.2) in the SPH simulations, Stacy, Bromm & Loeb (2011) have discussed the rotation velocity of the first stars, angular momentum transfer and the internal structure of the new-born protostars (see also Stacy et al. 2013, for the AREPO simulations). The central protostar rotates with a significant fraction of the Keplerian velocity. There is however scatter in the radial velocity, temperature, and accretion rate. In a recent study, Hirano et al. (2014) performed radiation hydrodynamical simulations to follow the evolution of 100 primordial protostars. Although their simulations were in 2D, they nicely compared the angular momentum of the cloud with the Pop III accretion rate. More recently, simulations and analytic models have shown the formation of the massive primordial stars in rapidly rotating disks in the presence of turbulence and UV backgrounds (Latif et al. 2013, and references therein). However, the extent to which the thermal and dynamical evolution of gas depends on the initial degree of rotation of the cloud has never been systematically tested. In addition, there is so far no clear understanding of how the cloud's rotation can regulate the concurrent heating and cooling process during the collapse.

The dependence of the resultant fragmentation on the cloud's initial rotation, however, has been shown in detail in previous studies (e.g., Machida et al. 2008; Saigo, Tomisaka & Matsumoto 2008). After performing a number of idealized numerical experiments, these parameterized studies have concluded that the formation of either binary or multiple systems depend highly on the initial rotation of the cloud. Nevertheless, these studies could not point out the influence on the thermal evolution of the primordial gas during collapse because their calculations adopted the model of equation of state (EOSs). In this work, we candidly scrutinize the role of initial rotation of the collapsing gas on the heating and cooling process that controls the chemothermal evolution of gas inside minihalos. In addition, we perform rigorous calculations in both the idealized as well as more realistic cosmological minihalos to thoroughly analyze the evolution of gas particles and their physical properties. This unique approach thus enables us to investigate in detail the thermal, chemical, and dynamical evolution of the baryonic matter in a full 3D simulation of Pop III collapse

to understand better the physical process and the resulting fragmentation behavior that occurs once the first object is formed. Finally, we address important issues, such as the relation of the physical property and accretion phenomenon of the protostars on the initial rotation of the collapsing core. We also discuss the possibility of survival of Pop III stars until today.

The paper is organized in the following manner. In §5.2 we describe the numerical setup of the simulations and the initial conditions. In §4.3 we briefly discuss the relevant physical concepts of the problem with an emphasis on the heating and cooling process that determines the temperature evolution. The details of the velocity structure are outlined in §4.4. We discuss the accretion phenomenon comprehensively, followed by the implication of this study for the fragmentation of primordial gas in §4.5. The long-term evolution of protostars are contoured in §4.6. We summarize the main points and draw our conclusions in §5.4.

4.2 Simulations

In order to follow the gravitational collapse, one needs to ensure that the gas evolution in the simulations should not depend on the choice of minihalos. We therefore use two completely different numerical setups: minihalos from the cosmological simulations of Greif et al. (2011) obtained from the hydrodynamic moving mesh code AREPO (Springel 2010) and the artificial minihalos with an initially uniform density distribution of gas particles. In the following, we describe the initial condition and setup of the simulations.

To investigate the cosmological minihalos, we use snapshots at the epoch when the central number density is just below 10^6 cm^{-3}, the onset of the crucial three-body H_2 formation reaction. The mesh-generating points of AREPO can be interpreted as the Lagrangian fluid particles, which is the basic characteristic of the GADGET-2 SPH code (Springel 2005). At this time, the minihalos contain masses of 1030 $M_\odot$ and 1093 $M_\odot$ with maximum central temperature of 469 K and 436 K, respectively. The complete physical nature of these minihalos (e.g., number density (n), initial rotation (β_0), maximum and minimum temperature, etc) is summarized in Table 4.1. We use

the AREPO output of these minihalos (MH-1 and MH-2 from Greif et al. 2011) as the initial conditions for our GADGET-2 implementation. Because of the conversion from the moving mesh to the SPH formalism (see, e.g., Smith et al. 2011; Dutta, Nath, Clark & Klessen 2015, we denote the minihalos as CH1 and CH2 for the GADGET-2 execution. The numerical resolution for CH1 and CH2 in SPH GADGET-2 simulations (for 100 SPH particles) is $\sim 10^{-2}\ M_{\odot}$.

For the artificial setup, we use the initial conditions that permit us to carry out a set of methodical numerical experiments. The randomly distributed gas particles have been settled using the periodic boundary conditions in a box. During this initial phase, we keep the gas temperature fixed and do not follow the primordial chemical network. Once the gas particles are settled, we are in a position to perform the simulations for the collapse of gas due to self-gravity.

The gas particles are initially uniformly distributed in a spherical cloud of size $R_0 \sim 2.7$ pc and a total mass of $M = 2982\ M_{\odot}$. The number density is $n = 10^3$ cm^{-3} and the temperature $T = 200$ K. These initial conditions are equivalent to the primordial gas clumps that collapse (see, e.g., Abel, Bryan & Norman 2002; Yoshida et al. 2006). All clouds are modeled with 5 million SPH particles, and the mass of a single SPH particle is $m_{\rm SPH} = 5.9 \times 10^{-4}\ M_{\odot}$. Therefore, the numerical resolution (roughly 100 SPH particles) is 0.06 $M_{\odot}$. The free-fall time for the uniform density distribution is $t_{\rm ff} = \sqrt{3/32\pi G\rho} = 1.37$ Myr and the sound crossing time is $t_{\rm sc} \approx 5$ Myr. As the free-fall timescale is shorter than the sound-crossing timescale, the clouds immediately start to collapse under their self-gravity. The clouds are then given different degrees of solid body rotation and are not subject to the internal turbulent motions. The strength of rotational support can be described by the β_0-parameter (Sterzik, Durisen & Zinnecker 2003),

$$\beta_0 = \frac{E_{\rm rot}}{E_{\rm grav}} = \frac{R_0^3 \Omega^2}{3GM}, \tag{4.1}$$

where Ω is the angular velocity, and $E_{\rm rot}$ and $E_{\rm grav}$ are the magnitudes of the rotational and the gravitational energies, respectively. We perform ten different numerical experiments with $\beta_0 = 0.0, 0.005, 0.007, 0.01, 0.02, 0.04, 0.05, 0.07, 0.1, 0.2$.

Table 4.1: Physical properties of the cosmological minihalos are summarized:

Halo properties	CH1	CH2
n (cm^{-3})	10^6 (max) 71 (min)	10^6 (max) 85 (min)
T (K)	469 (max) 59 (min)	436 (max) 54 (min)
mass ($M_\odot$)	1030	1093
n-SPH	690855	628773
resolution ($M_\odot$)	1.3 $\times 10^{-2}$	1.4 $\times 10^{-2}$
β_0	0.035 (max) 0.025 (min)	0.042 (max) 0.03 (min)

Note: n denotes the number density, T the temperature, n-SPH the number of SPH particles and β_0 the rotation parameter, respectively. The numerical resolution is calculated for the 100 SPH particles.

As the collapse progresses in the central region of the cloud, it is extremely difficult to simulate the higher density regime because of shorter timescale. To overcome this problem, we use the sink particle technique in which the high-density region is replaced by a single sink particle with appropriate boundary conditions (see, e.g., Bate, Bonnell & Price 1995; Krumholz, McKee & Klein 2004; Jappsen et al. 2005). The sink particle can then be assumed to be (or at least approximated by) a growing protostar. The density threshold for the sink particles to form is set as the number density of 5 $\times 10^{13}$ cm^{-3}, at which point the gas has a temperature of $\sim$1000 K. The sink particle can accrete gas particles within its accretion radius $r_{\rm acc}$, which we fix at 6 AU, the Jeans radius at the density threshold for sink creation. The corresponding Jeans mass for both the cosmological as well as the artificial clumps is 0.06 $M_\odot$, so we can resolve both the cosmological and artificial minihalos. The softening parameter of the sinks is 1.2 AU. In order to avoid spurious formation of new sink particles out of the gas, the sink particles is prevented further from forming within $2\,r_{\rm acc}$ of one another.

We follow Clark et al. (2011a) for the implementation of the external pressure term and a time-dependent primordial chemical network. To model a constant pressure boundary, we used a modified version of the GADGET-2 momentum equation,

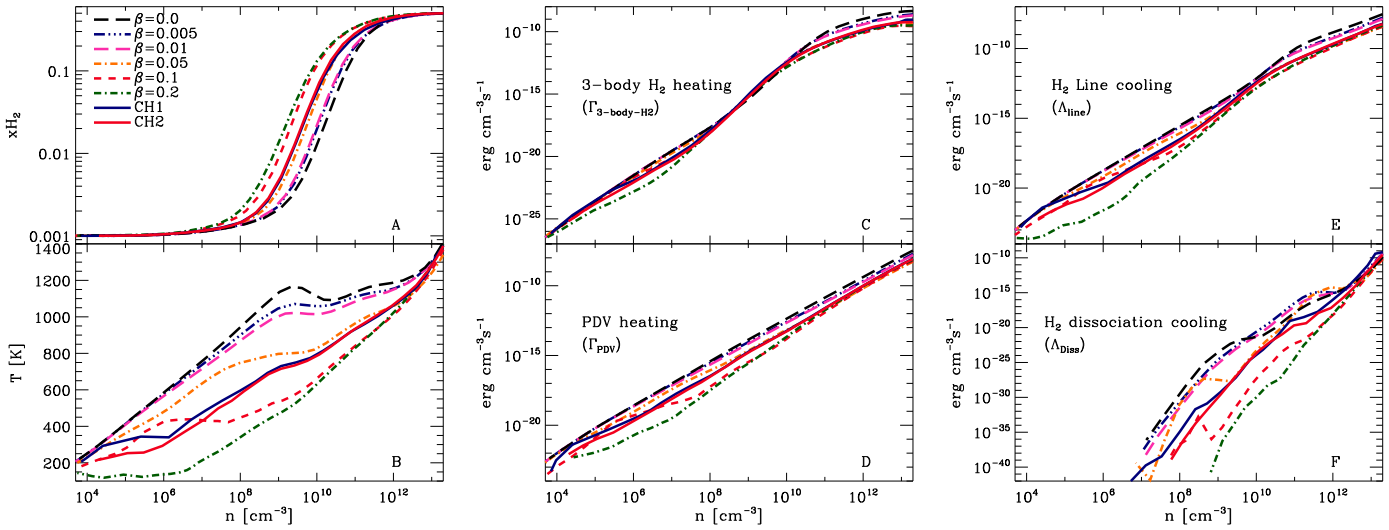

Figure 4.1: Radial logarithmic binned, mass-weighted averages of the H_2 fraction (A), temperature (B), and various heating and cooling rates (C to F) are plotted as a function of density for different degrees of initial rotation β_0, just before the formation of the first sink.

$$\frac{\mathrm{d}v_i}{\mathrm{d}t} = -\sum_j m_j \left[f_i \frac{P_i}{\rho_i^2} \nabla_i W_{ij}(h_i) + f_j \frac{P_j}{\rho_j^2} \nabla_i W_{ij}(h_j) \right], \tag{4.2}$$

where the contribution from the external pressure ($P_{\rm ext}$) is subtracted from both P_i and P_j (i.e., P_i and P_j are replaced by $P_i - P_{\rm ext}$ and $P_j - P_{\rm ext}$, respectively). All quantities have their usual meaning. The chemical network includes primordial hydrogen, helium, and deuterium to model the chemical and thermal evolution of the metal-free gas inside minihalos. The details of all the chemical reactions are given in Glover & Abel (2008) and references therein. We adopt the intermediate three-body H_2 rate coefficient $7.7 \times 10^{-31} T^{-0.464}$ cm^6 s^{-1} proposed by Glover (2008).

4.3 Heating and cooling rate

In this section, we investigate the cooling and heating mechanism associated with the emission, chemical reactions and gas contraction during the collapse of the cloud

under its own gravity. The differences in the cooling and heating rates can force the gas to choose different paths for its thermodynamic evolution.

If we assume that the gas density (ρ) evolves with the free-fall time ($t_{\rm ff}$) of the gas, i.e., $\mathrm{d}\rho/\mathrm{d}t = \rho/t_{\rm ff}$ (see, e.g., Omukai 2000; Glover & Savin 2009), the thermal evolution can then be followed by solving the energy equation

$$\frac{\mathrm{d}\epsilon}{\mathrm{d}t} = \frac{p}{\rho}\frac{\mathrm{d}\rho}{\mathrm{d}t} - \Lambda + \Gamma, \tag{4.3}$$

where ϵ is the energy per unit volume in the gas, and Λ and Γ are the cooling and heating rates, respectively, in units of erg s^{-1} cm^{-3}. Figure 4.1 shows the physical conditions in the gas once the central region has collapsed to a density of $\sim$5 $\times$ 10^{13} cm^{-3}, i.e., just before the first sink formation. The panels show mass-weighted averages of the properties of individual SPH particles within the radial logarithmic bins.

The three-body H_2 formation heating rate provides chemical heating associated with the release of 4.48 eV each time a H_2 molecule forms. Because the H_2-fractions are almost similar (Fig. 4.1A), there is no consequential effect of the three-body H_2 heating on the cloud's initial rotation (Fig. 4.1C). However, we find that there are substantial temperature differences between the clouds (Fig. 4.1B). For example, the temperature of the cloud with $\beta = 0.2$ is almost 40-60% lower than that with $\beta_0 = 0.005$. This is because a higher degree of the rotational support slows down the contraction and reduces the amount of compressional heating (Fig. 4.1D). Thus, the cloud with $\beta = 0.2$ has a temperature of roughly $T \leq 200$ K due to a slower collapse and, hence, less efficient compressional heating, whereas the temperature is nearly 1100 K in case of $\beta = 0.0$ or $\beta = 0.005$.

The rapid conversion of atomic to molecular hydrogen during the three-body reaction cools the gas less than the free-fall time and hence causes chemothermal instability (Dutta 2015). At high densities the heating rate is as high as the line-cooling rate (Fig. 4.1E), however, again with slight differences over the range of β_0 modeled. At equilibrium, the formation rate is balanced by the dissociation, and hence the dissociation cooling rate behaves in the same way with density as the heating rate.

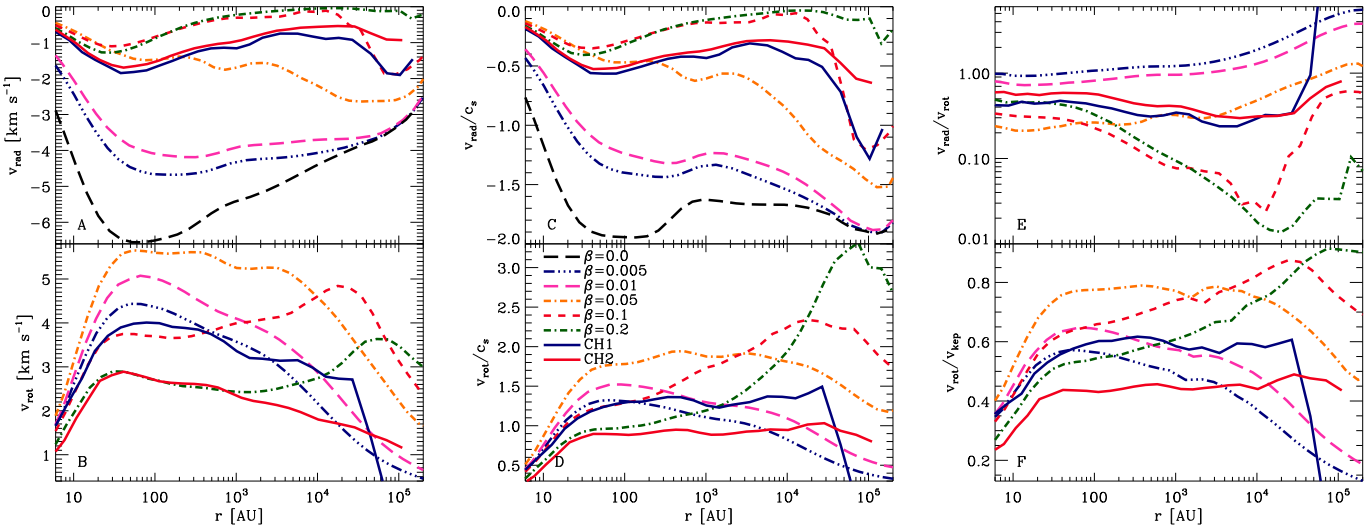

Figure 4.2: Radial logarithmic binned, mass-weighted averages of the radial velocity (A), rotational velocity (B), radial velocity over sound speed (C), rotational velocity over sound speed (D), rotational velocity over Keplerian speed (E), and radial velocity over rotational velocity are plotted as a function of radius, just before the first protostar forms. The initial strength of rotation introduces a scatter in the velocity.

The dissociation cooling rate varies between clouds, with that for $\beta_0 = 0.005$ nearly 10 orders of magnitude higher than for the $\beta_0 = 0.2$ model (Fig. 4.1F) in the density range where the three-body reaction dominates. We, therefore, conclude that it is indeed the compressional heating (pdV) that determines the thermal evolution of gas, which strongly depends on the initial degree of rotation (β_0).

At this point, it is worth pointing out that the temperature evolution of the cosmological minihalos are similar to that of the idealized cases. As expected, both CH1 (with $\beta_0 \approx 0.035$) and CH2 (with $\beta_0 \approx 0.042$) have the temperature variation that falls in between the highest and lowest β_0 modeled throughout the density space. This also confirms that our varied parameter study with idealized clumps actually represents the cosmological initial conditions of the minihalos.

4.4 Velocity structure

In this section, we study the dynamics of the gas particles that can arise as a result of the chemical and thermal evolution of the clouds. We therefore take a closer look at the velocity of the gas associated with the cloud collapse. The radial profiles of the gas show the mass-weighted averages within logarithmic bins and are taken just before the formation of the first sink.

We find that there are considerable differences in radial velocities between the clouds (Fig. 4.2A). The radial velocity of the cloud with $\beta_0 = 0.005$ is almost 30-40% higher than the cloud with $\beta_0 = 0.2$. This is consistent with the fact that a lower rate of compressional heating for the gas of the collapsing core implies a lower radial velocity, which is nearly comparable with the sound speed (Fig. 4.2C).

In order to quantify the degree of rotational support, we plot the rotational velocity (Fig. 4.2B) and the ratio of the rotational velocity ($v_{\rm rot}$) to the Keplerian velocity ($v_{\rm Kep}$), defined as $v_{\rm K} = \sqrt{GM_{\rm enc}(r)/r}$, where $M_{\rm enc}(r)$ is the mass enclosed within the radius r (Fig. 4.2F). We find that the rotational speed for all β_0 modeled is well below that required for rotational support by a factor of 5 to 7. This is consistent with previous cosmological simulations (e.g., Yoshida, Omukai & Hernquist 2008; Turk, Abel & O'Shea 2009), which argued that the collapsing gas cloud has the ratio $v_{\rm rot}/v_{\rm Kep} \sim 0.5$.

For the $\beta_0 = 0.2$ case, the rotation speed varies between 0.3 and 0.9 times the Keplerian velocity, indicating that this cloud has gone through an efficient phase of angular momentum redistribution (Dutta 2016b). However, for $\beta_0 > 0.05$ the collapsing cloud is almost completely rotationally supported throughout and the gas at higher densities is relatively cold. All clouds are consequently sub-Keplerian, and the radial velocities for all clouds are comparable to the rotational velocities within 100 AU (Fig. 4.2E). From this discussion, we can infer that the cloud with higher rotation transfers the angular momentum more efficiently and hence becomes Keplerian in the outer regime of the collapsing core (for instance, $v_{\rm rot} \sim v_{\rm Kep}$ for $r \geq 10^4$ AU for $\beta_0 = 0.2$). Thus the outer regime, which is likely to form a Keplerian disk due to rotation, becomes unstable enough from accreting mass and, consequently, has higher

chance to fragment (as we see in the next section). We conclude that the cloud's initial rotation plays a pivotal role in the dynamical evolution of the gas by affecting the amount of rotational support even at later stages of the collapse.

4.5 Mass accretion and fragmentation

During collapse, the angular momentum is transported to smaller scales, resulting in the formation of rotationally supported disk-like structures (Stacy, Bromm & Loeb 2011; Greif et al. 2012). However, the rotation is not sufficient to hold the collapse of the disk, which then fragments into multiple objects (Clark et al. 2011; Dutta, Nath, Clark & Klessen 2015). We thus gauge the accretion and gas instability carefully, as predicted by the properties of the gas, to check whether there is any hint of fragmentation already present before the formation of the first sink.

We follow Abel, Bryan & Norman (2002) to study the mass accretion rate, estimated as $\dot{M}(r) = 4\,\pi\,r^2\,\rho(r)\,v_{\rm rad}(r)$, as a function of radius for different degrees of initial rotation (Fig. 4.3A). We also define the accretion time, $t_{\rm acc} = M_{\rm enc}(r)/4\,\pi\,\rho\,v_{\rm rad}\,r^2$. For all simulations, $\dot{M}$ has a maximum at ∼20-40 AU. Given that H_2 line cooling becomes optically thick at the corresponding densities, $\dot{M}$ for all simulations converges in this range, as the gas looses its ability to cool efficiently. We would, however, like to point out that the scale, where $\mathrm{d}M/\mathrm{d}t$ becomes maximum, may slightly change with the choice of density threshold for the sink formation. For example, if we choose $n \sim 10^{15}$ cm^{-3} for a sink particle to form, the collapse of the inner structure proceeds and hence the mass accretion rate reaches a maximum at ∼15-30 AU, depending on the initial degree of rotation. However, this is not a substantial issue compared to the overall thermal nature of the collapsing cloud. For slowly rotating clouds, the accretion rate is substantially higher (∼0.1 yr^{-1}) and the accretion time is on the order of free-fall time (Fig. 4.3C).

Since the collapsing core becomes Jeans unstable by accreting more and more mass, we check the strength of the gravitational instability by measuring the number of the Bonnor-Ebert masses ($M_{\rm BE}$) contained in the central dense volume (Ebert 1955; Bonnor 1956). We compute the Bonnor-Ebert masses (Abel, Bryan & Norman

2002) as

$$M_{\rm BE} = 1.18(c_s^4/G^{3/2})P_{\rm ext}^{-1/2} \approx 20 M_\odot T^{3/2} n^{-1/2} \mu^{-2} \gamma^2, \tag{4.4}$$

where c_s is the sound speed, $P_{\rm ext}$ is the external pressure that we assume to be equal to the local gas pressure, μ is the mean mass per particle, and $\gamma = 5/3$ is the adiabatic index, respectively. Within the central 10^4 AU regime, the enclosed gas mass for all values of β_0 contains a roughly equal number of Bonnor-Ebert masses, although with a factor of two between the highest and lowest values of β_0 (Fig. 4.3B). However, in the outer regime (i.e., $r \geq 10^4$ AU), the clouds with $\beta_0 = 0.1$ and $\beta_0 = 0.2$ contain roughly 7 and 10 Bonnor-Ebert masses respectively. This is because the higher rotating clouds become close to Keplerian in the outer regime (as seen in the previous section) and tend to form a disk-like structure. As the higher rotation obstructs the infalling gas particles, the disk gradually accumulates enough Jeans masses through accretion and becomes gravitationally unstable to fragmentation.

Alongside the Bonnor-Ebert analysis, we also compare all relevant timescales associated with the cloud collapse. Figure 4.3C represents the accretion timescale ($t_{\rm acc}$) over free-fall timescale ($t_{\rm ff}$). For a higher rotating cloud, the accretion time is much longer than the free-fall time. This is consistent with the above discussion and an alternate way to explain the mass accretion features of clouds with different β_0-models shown in Fig. 4.3A. In Fig. 4.3D, we consider the fragmentation timescale, defined as $t_{\rm frag} \equiv M_{\rm BE}/\dot{M}$ (e.g., Dopcke et al. 2013), and compare it with the free-fall timescale. We know that fragmentation generally occurs when the dynamical timescale of the central collapse becomes larger than the collapse timescale of individual density fluctuations. Here the free-fall timescale represents the dynamical timescale. In the outer regime ($r \geq 2 \times 10^4$ AU), which is likely to form a disk, the fragmentation time becomes shorter than the free-fall time, especially for higher rotating clouds. We conclude here that the clouds with larger β_0 collapse slowly from high rotation and tend to form a disk-like structure that becomes Keplerian and gravitationally unstable by accreting mass, heralding fragmentation.

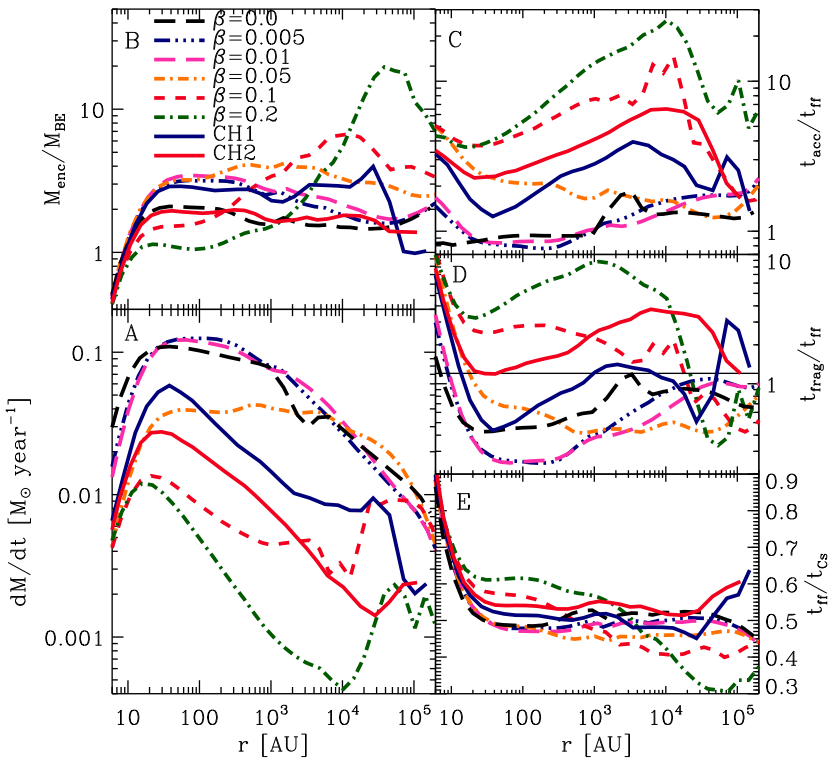

Figure 4.3: Radial logarithmic binned, mass-weighted averages of the mass accretion rate (A), the number of Bonnor-Ebert masses (B), the accretion time over free-fall time (C), the fragmentation time over free-fall time (D), and the free-fall time over sound crossing time (E) are plotted as a function of radius, just before the formation of the first sink.

4.6 Protostellar system

The study by Machida et al. (2008) shows that any fragmentation only takes place after the disk formation, and that clouds with higher β_0 tend to fragment at lower densities. We examine how the circumstellar accretion disk that formed in the idealized, as well as more realistic cosmological minihalos, becomes locally unstable and evolves for different degrees of initial rotation.

Figure 4.4 shows the column density and column-weighted temperature distribution in the inner 2000 AU at the end of the simulations. These images clearly reflect that all simulations fragment to form a small N-body system, comprised of secondary

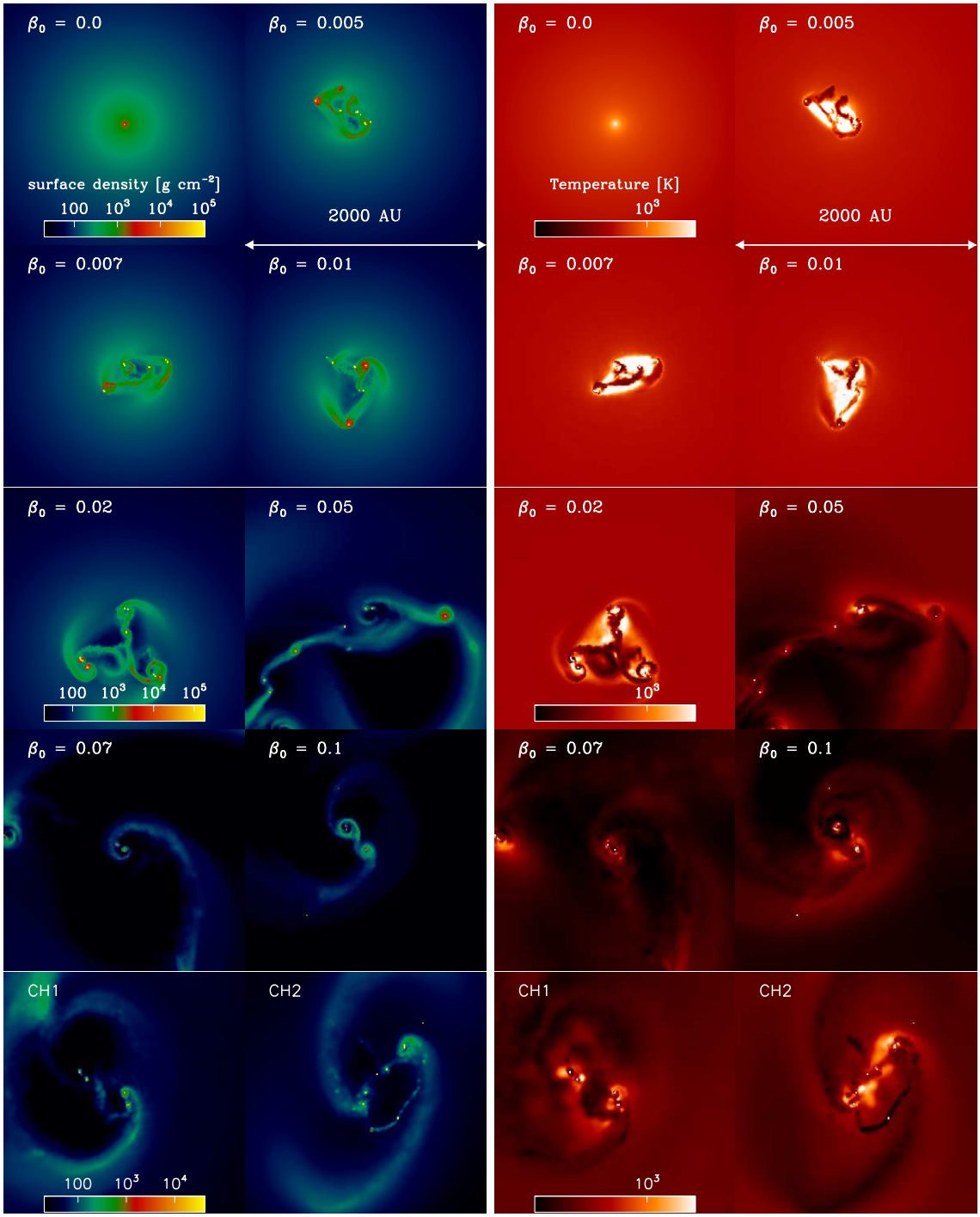

Figure 4.4: The column density and column-weighted temperature distribution in a region of 2000 AU centered around the first protostar for different strengths of the initial rotation of the cloud are shown when a total of $\sim 30\,M_\odot$ have been converted into, or accreted onto, sink particles.

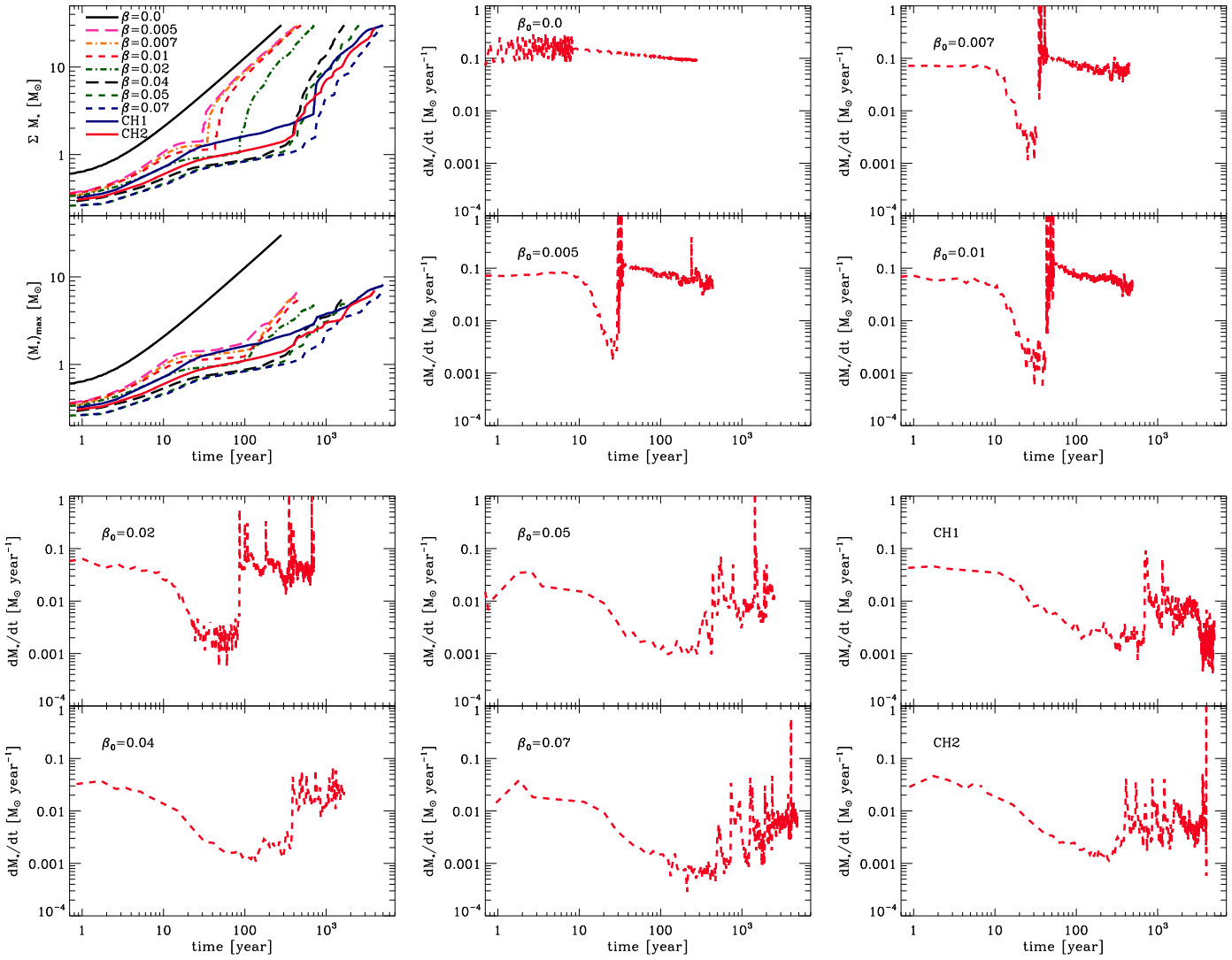

Figure 4.5: Time evolution of the protostellar system: total mass of all the sink particles and the most massive sink particle are plotted as a function of time (top left). Total mass accretion rate by all sink particles are shown as a function of time (for others rotation parameter β_0; same as Fig. 4.3A). The cloud with zero rotation attains 30 $M_\odot$ within a few hundred years after the formation of the first sink particle. The rotationally supported cloud takes $\sim$ 100 – 1000 years, depending on the initial strength of rotation (β_0). The mass accretion rate decreases with time until further sink particles form.

protostars, within the time in which ∼30 $M_\odot$ of material are accreted onto the sink particles. It is not surprising that clouds with a higher level of rotational support exhibit the disk-like structure on several scales within the central region, whereas slowly rotating clouds are more likely to be centrally condensed.

The top left panel of Fig. 4.5 shows the time evolution of the total mass accreted onto all the sinks (ΣM_*) and the maximum sink mass ($M_{*\rm max}$) in the period over which the sink formation occurs. We find that the cloud with zero rotation attains the 30 $M_\odot$ within a few hundred years after the formation of the first sink particle, whereas rotationally supported clouds take ∼100–1000 years, depending on the initial strength of rotation. Figure 4.5 also shows the time evolution of the total mass accretion rate ($\mathrm{d}M_*/\mathrm{d}t$) onto all the sinks (same as Fig. 4.3A) for different values of β_0. As expected, the mass accretion rate is larger for the slowly rotating clouds. In each case, $\mathrm{d}M_*/\mathrm{d}t$ decreases with time until further sink particles form, and then the total accretion rate increases again, however, this time with large temporal variations. The mass accretion rate for the idealized cloud with $\beta_0 = 0.04$ is similar to that of the cosmological minihalo CH2, which has a rotation parameter $\sim\beta_0 = 0.042$. This again confirms that our idealized clumps with varying β_0 can actually be the representatives of cosmological initial conditions to investigate the thermodynamical evolution of gas and the resulting fragmentation behavior of the sinks.

Figure 4.6A shows the number of sinks for different values of β_0, with rotationally supported clouds fragmenting the most. This is consistent with the recent study by Becerra et al. (2015), who have used AREPO simulations to investigate the dependence of the high accretion rate and efficient cooling of the gas on the fragmentation of the disk. However, Fig. 4.6A shows some scatter in the numbers, indicating the presence of statistical fluctuations that can be removed by pursuing more realizations to achieve a desired degree of accuracy. Figure 4.6B shows the time taken for all the clouds to accumulate ∼30 $M_\odot$. As expected, higher rotating clouds take longer compared to their slowly rotating counterparts. Figure 4.6C shows the distance at which the primordial protostars form from the center of the cloud. The red line represents the mean distances of all protostars ($R_{\rm dist}$), which follows a power-law relationship with the cloud's initial rotation, $R_{\rm dist} \propto \beta_0^{3/4}$. The protostars of the slowly rotating clouds

form near the center ($\leq$ 300 AU), while the others spread over larger distances of 5000 AU, as the conservation of angular momentum acts to move protostars to larger radii.

Another trend we find in our simulations is that a number of protostars are ejected from the central gas cloud, as seen in cosmological simulations (Greif et al. 2011). Although the resolution used in those studies was higher than our resolution, we still find ejection from the cluster. Figure 4.7 shows the radial velocity and the ratio of the radial velocity to the escape velocity for all protostars. The position of the sinks is measured from the center of mass of all the sinks. The escape velocity of the sinks is defined as $v_{\rm esc} = \sqrt{2GM_{\rm enc}(r)/r}$, where $M_{\rm enc}(r)$ is the total mass (gas + sinks) that is enclosed within the radius r. The radial velocities of the sinks formed with lower β_0 are below that required to be kicked out of the cluster. They tend to remain within the cluster and continue to accrete. For faster-rotating clouds, some protostars move from the cluster with radial velocities exceeding the escape velocity. There is, therefore, a greater chance that some protostars will be ejected, opening up the possibility that they could survive until the present day.

At this point we would like to point out that we have not mentioned the behavior of sinks for the $\beta_0 = 0.2$ case. The thermodynamical evolution of this cloud is considerably different from other cases, so it is important to compare the fragmentation behavior of $\beta_0 = 0.2$ cloud with others. However, because of very fast rotation it has been extremely tough to run the simulation up to the point where the total mass of all sinks reaches $\sim$30 $M_\odot$. The simulation with $\beta_0 = 0.2$ stops much before compared to other simulations. For instance, simulation with $\beta_0 = 0.2$ stops when the total mass of sinks is only around 3–4 $M_\odot$ (and to reach up to that epoch of time; it takes around one month to run on a supercomputer that is based on graphical processing units, HPC–GPU Cluster Kolob). This is usually expected as the fast rotation can impede the collapse. We find a limiting value of $\beta_0 = 0.1$ for the simulation to run up to the epoch when the mass of sinks attains a value of 30 $M_\odot$. However, Figs. (4.4–4.6) still allow us to extrapolate and predict the expected results.

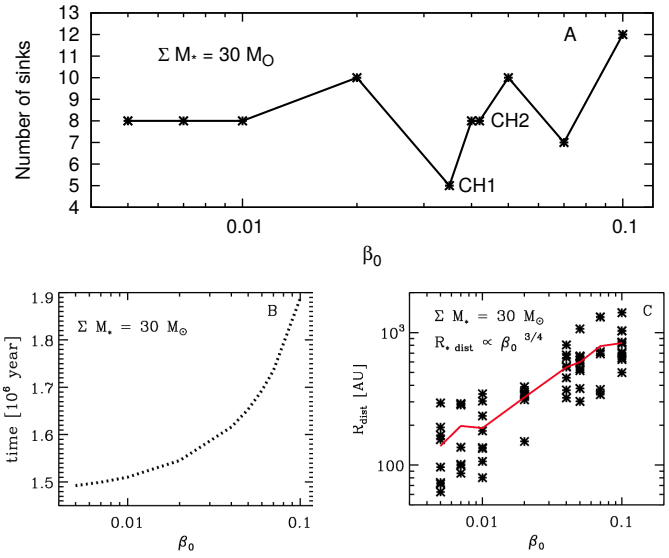

Figure 4.6: The fragmentation behavior is plotted for different degrees of initial rotation at the epoch when stellar system accretes $\sim 30\ M_{\odot}$. The number of sinks (A), time taken to accrete $\sim 30\ M_{\odot}$ (B) and the position of the sinks ($R_{\rm dist}$) from the center of mass is shown in (C) as a function of the rotation parameter β_0.

4.7 Summary and discussion

We have minutely investigated the dependence of the thermodynamical evolution of primordial star-forming gas on the initial degree of rotation of the cloud, and analyzed its influence on the resulting fragmentation of the circumstellar accretion disk. For this purpose, we performed a set of three-dimensional hydrodynamical simulations of Pop III gas collapse to pursue a systematic parameter study, specified by β_0, which spans two orders of magnitude for the amount of initial rotation, including two simulations runs with realistic cosmological initial conditions.

The cloud's initial strength of rotation introduces a significant impact on the intricate combinations of the heating and cooling process, leading to a scatter in the temperature evolution of the collapsing gas. Clouds with slower rotation collapse faster and get heated as a result of the compressional heating. We also find that the dynamical evolution of the gas strongly depends on the initial strength of rotation. Clouds with higher rotation form a Keplerian disk that becomes gravitationally unstable by

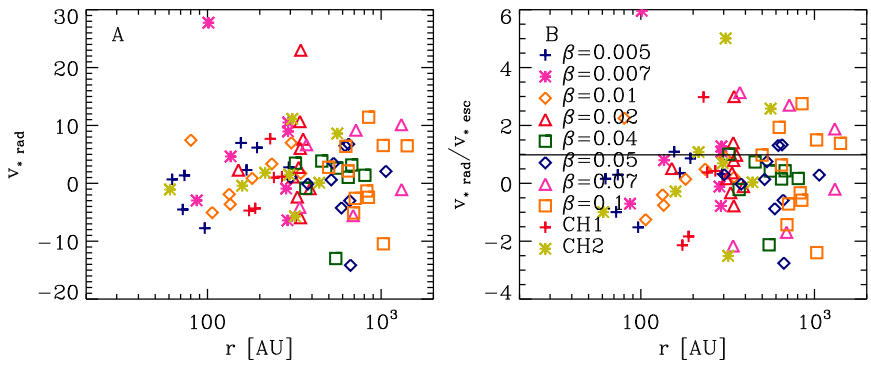

Figure 4.7: Radial velocity (A) and the ratio of the radial velocity to the escape velocity (B) of sink particles for different values of β_0 are plotted as a function of radius, at the epoch when the stellar system has accreted $\approx 30\ M_\odot$. Some protostars with higher β_0 move away from the cluster, with the radial velocity exceeding the escape velocity.

accreting the infalling mass. Therefore, any change in the thermodynamical evolution introduces substantial difference in the number of Jeans mass, which determines the susceptibility to the fragmentation of the gas between the clouds with highest and lowest initial rotation.

In summary, a higher degree of rotation can hinder the infall, lead to a cooler gas, and result in more fragmentation. In addition, we find that the protostars with higher rotational support have larger spiral arms with lower accretion rates. We also point out that the newborn protostars are distributed in such a way to conserve the angular momentum, and some of them could have survived until today if they were of sufficiently low mass.

We conclude that the initial conditions of the primordial gas in the minihalos should be chosen scrupulously so as to simulate the long-term evolution and final fate of the primordial stars.

Despite considerable computational efforts involved, we emphasize that we cannot accurately predict the final mass of the primordial protostars. We have neglected the effect of the magnetic fields, which can be important in minihalos (Machida, Matsumoto & Inutsuka 2008; Sur et al. 2010; Schleicher et al. 2010). Recent cosmological simulations show the importance of the amplification of even small seed fields

(Federrath et al. 2011; Schober et al. 2012). In addition, the radiative feedback can significantly affect the thermal as well as chemical evolution of the gas (Wise & Abel 2008; Whalen, Hueckstaedt & McConkie 2010; Hosokawa et al. 2011), which is not included in our simulations. Notwithstanding, our approach to the problem enables us to provide good estimates for the overall trend of the accretion rate, thermodynamical evolution, and fragmentation behavior of gas in the rotating clouds in which we are particularly interested. Recent radiation hydrodynamic simulations (Hirano & Yoshida 2013; Greif 2014) demonstrated the effect of UV radiative feedback on the mass accretion, thus constraining the mass spectrum of the first stars (Susa 2013). Moreover, there is still a discrepancy regarding the three-body H_2 rate coefficient (Turk et al. 2011; Bovino, Schleicher & Grassi 2014; Dutta, Nath, Clark & Klessen 2015). However, the recent study by Forrey (2013) provides the currently best available rate that is in good agreement with Palla, Salpeter & Stahler (1983) at high temperatures and Abel, Bryan & Norman (2002) at lower temperatures. It is therefore of strategic interest to accurately simulate the formation of the first stars in the universe with the best available rates, inclusion of the magnetic fields, and radiative feedback in the next-generation avant-garde SPH codes.

Chapter 5

Angular momentum distribution during the collapse of primordial star-forming clouds

It is generally believed that angular momentum is distributed during the gravitational collapse of the primordial star forming cloud. However, so far there has been little understanding of the exact details of the distribution. We use the modified version of the GADGET-2 code, a three-dimensional smoothed-particle hydrodynamics simulation, to follow the evolution of the collapsing gas in both idealized as well as more realistic minihalos. We find that, despite the lack of any initial turbulence and magnetic fields in the clouds the angular momentum profile follows the same characteristic power-law that has been reported in studies that employed fully self-consistent cosmological initial conditions. The fit of the power-law appears to be roughly constant regardless of the initial rotation of the cloud. We conclude that the specific angular momentum of the self-gravitating rotating gas in the primordial minihalos maintains a scaling relation with the gas mass as $L \propto M^{1.125}$. We also discuss the plausible mechanisms for the power-law distribution.

5.1 Introduction

The significant progress in the theoretical as well as numerical calculations has provided a great stride in our understanding of the history of the universe, especially the transition period from the 'Cosmic Dark Ages' to the first source of light to the present-day clumpy structure of the universe (Madao 2000; Barkana & Loeb 2001; Heger & Woosley 2002; Umeda & Nomoto 2003; Schneider et al. 2003; Frebel et al. 2005). In last two decades, there have been extensive studies on the hierarchical structure formation that eventually leads to the collapse of the first gravitationally and thermally unstable primordial gas clouds (Reed et al. 2005; Ciardi & Ferrara 2005; Yoshida et al. 2006; O'Shea & Norman 2007). It has been shown that the angular momentum of the dark matter (DM) and baryons become comparable during virialization (Wise & Abel 2007). The physics that determines the collapse is extremely complex along with a complicated chemical network, and is intrinsically multidimensional, nonlinear and not in equilibrium (Glover & Abel 2008; Whalen et al. 2008; Bromm, Yoshida, Hernquist & McKee 2009; Hosokawa et al. 2011; Johnson, Dalla & Khochfar 2013).

One of the interesting physical problems is the distribution of the angular momentum of the baryons that have collapsed gravitationally within minihalos (Larson 1969, 1972; Silk 1977; Norman, Wilson & Barton 1980; Couchman & Rees 1986). This process ultimately leads to the formation and evolution of the very first stars in the universe, the so-called Population III (or Pop III) stars (e.g., Haiman et al. 1996; Tegmark et al. 1997; Omukai & Nishi 1998). Numerical computations using various methods (primarily Lagrangian and Eulerian code) make it possible to study the gas dynamics with higher spatial resolution (e.g., Bromm, Coppi & Larson 1999; Abel, Bryan & Norman 2000). These calculations conclude that the angular momentum of the continually collapsing core is just a fraction of the total angular momentum of the cloud in which the high-density core forms (Abel, Bryan & Norman 2002; Fisher 2004; Jappsen & Klessen 2004). Clearly angular momentum must be redistributed during the star formation (O'Shea & Norman 2008; Yoshida, Omukai & Hernquist 2008; Turk, Abel & O'Shea 2009).

The angular momentum in protogalaxies also has substantial effect on the temperature evolution (Vasiliev, Vorobyov & Shchekinov 2010). They concluded that the increase of rotational angular momentum of the gas results in cooling of the gas to a temperature less than 100 K. It is therefore obvious that the existence of initial angular momentum can delay the formation of the primordial stars. Even the efficiency of fragmentation and the star formation rate in primordial gas becomes sensitive to the angular momentum (Bromm, Coppi & Larson 2002). The same conclusion has been drawn by Dutta et al. (2012) showing that the cloud with higher angular momentum leads to a lower gas temperature compared to their slowly rotating counterparts. More recently, the angular speed of the first stars has been investigated thoroughly using the sink particles method (a computational technique in which a certain high density regime is considered as a growing protostars that can accrete gas particles) in cosmological simulations by Stacy, Bromm & Loeb (2011). Although angular momentum is conserved during the collapse of a rotating gaseous cloud, a small fraction of the cloud's mass at the center can collapse to stellar densities, leaving behind the rest of cloud in an extended rotationally supported envelope that fragments (Clark et al., 2011). The fraction of the collapsing cloud that ends up in a star or stellar system depends on the amount of angular momentum transferred outward during the collapse (e.g., Greif et al. 2012; Stacy & Bromm 2013).

The recent simulations, e.g., using the moving mesh code AREPO by Greif (2015) and using smoothed particle hydrodynamics (SPH) by Dutta (2016a) have addressed important issues such as transfer and redistribution of the angular momentum while describing the velocity structure, accretion and thermal evolution of gas in a number of minihalos. The analytic models for the rapidly rotating disks in the presence of turbulence and UV backgrounds have been discussed in a series of papers (Latif & Schleicher, 2015, and references therein). In addition, there is strong indication of the dependency of the angular momentum on the Pop III accretion rate in the current literature (Hirano et al. 2015). However, so far there has been little understanding on the basic characteristic of cloud's angular momentum distribution and evolution during the gravitational collapse of the primordial star forming gas. The extent to which the angular momentum of the cloud depends on the initial strength of rotation

has never been systematically tested. Moreover, there is still ambiguity of the basic physical mechanism that is responsible for the distribution of angular momentum in primordial clouds. In our recent study, we have taken care to address the influence of the initial rotation of the primordial cloud on the thermal, chemical and dynamical evolution that results in the fragmentation of the disk (Dutta 2016a). In this work, we revisit the physics of gravitational collapse of the primordial gas with a particular focus on the angular momentum profile in the evolutionary stage. Our approach to investigate the gas evolution is different from the previous studies in the sense that we scrutinize the angular momentum distribution for a large set of simulations with a varied initial degree of rotation of the gas clump and compare the result with more realistic cosmological simulations that was based on different numerical formalism. We have studied the gas collapse till it attains the protostellar densities.

In the next section §5.2, we briefly outline the numerical set-up of simulations and initial conditions. We then discuss the relevant physical concept of the problem with an emphasis on the origin and distribution of the angular momentum of the collapsing gas in §5.3. We draw our conclusions in §5.4.

5.2 Simulations

To investigate the angular momentum distribution, we use a simple and straightforward numerical set-up where the gravitationally unstable gas clump is assumed to be spherical of size ∼2.7 pc. For simplicity, we assume that gas particles are uniformly distributed with an initial number density $n_0 = 10^3$ cm^{-3} and temperature $T_0 = 200$ K. These values are consistent with the primordial gas cloud at redshift $z \geq 20$ (Abel, Bryan & Norman 2002; Bromm & Larson 2004).

Initially the gas clump contains only atomic hydrogen that will collapse only if the gravitational potential energy of the cloud is greater than the net kinetic energy. With no external source of cooling, the above criteria is fulfilled because the free-fall time ($t_{\rm ff} = \sqrt{3\pi/32G\rho} = 1.37$ Myr) is shorter than the sound-crossing time $t_{\rm sc} \approx 5$ Myr. The gas cloud therefore inevitably starts to collapse under the self-gravity. We use 5 million SPH particles to model the gas distribution in the cloud of total mass

of $M \sim 3000\ M_{\odot}$. The numerical resolution (for 100 SPH particles) is 0.06 $M_{\odot}$.

With this set-up, the artificial clump is given initial angular momentum that can be obtained from the rotational ($E_{\rm rot}$) and the gravitational ($E_{\rm grav}$) energies of gas particles. We follow Sterzik, Durisen & Zinnecker (2003) to model the angular velocity of the cloud in which the decisive parameter β_0, where $\beta_0 = E_{\rm rot}/E_{\rm grav} = R_0^3\Omega_0^2/3GM_0$, sets the strength of rotational support of the gas clump. Here R_0 and Ω_0 are the radius and angular velocity of the gas clump. We perform six numerical experiments with varied β_0 parameters, whose magnitude spans two orders of magnitude.

We take care to ensure that our investigation is not biased by the artificial configuration of the gas clump. Hence we investigate the angular momentum distribution in two different minihalos (CH1 and CH2 of Dutta, Nath, Clark & Klessen 2015) obtained from cosmological simulations of the hydrodynamic moving mesh code AREPO (Springel 2010). We implement these realistic minihalos in our modified SPH GADGET-2 code (Springel 2005). We here mention that although both the codes, i.e., AREPO and GADGET-2 use different approach in solving hydrodynamics equations, both of them basically follow the Lagrangian formalism. This enables us to use the minihalos from the unstructured moving mesh into SPH configuration.

We summarise here the detailed configuration and initial conditions of these minihalos (see table 1 of Dutta 2016a for the detailed configuration of the halos). The gas density of both minihalos increases towards the centre of cloud and has a maximum value $n \sim 10^6$ cm^{-3}. We have chosen this limit because the gas will go through a rapid phase of transition at density $n \geq 10^6$ cm^{-3} via three-body H_2 formation reactions 1.5,1.6 (Palla, Salpeter & Stahler 1983). We can therefore simulate the crucial transformation of the atomic to molecular hydrogen as the collapse proceeds to higher density. The rapid formation of the molecular hydrogen cools the gas very efficiently and initiate chemothermal instability (Dutta 2015). Although the rate coefficient for this reaction is highly uncertain, we choose the intermediate one that is $7.7 \times 10^{-31} T^{-0.464}$ cm^6 s^{-1} (Glover 2008). The minihalos CH1 and CH2 contains gas mass of 1030 $M\odot$ and 1093 $M\odot$ respectively. The temperature at the center of both minihalos has a maximum value ∼450 K, while at the periphery it is ∼50 K. With altogether six million SPH particles in each of our simulations, we are able to resolve

the angular velocity of the gas significantly better than in the SPH models of our previous study. The numerical resolution of our simulations for both minihalos are of the order of 0.01 $M\odot$. The initial rotation of minihalos, defined by the spin parameter (β_0), is 0.035 (for CH1) and 0.042 (for CH2) respectively. So the realistic minihalos falls intermediate compared to the idealized gas clump where we simulate the gravitational collapse of solid body with β_0 = 0.0, 0.005, 0.01, 0.05, 0.1 and 0.2 respectively.

The chemical network for primordial collapse is extremely complex with primordial hydrogen, helium and deuterium mixing in a different ways to contribute toward the thermal, chemical and dynamical evolution of gas. We follow Dutta, Nath, Clark & Klessen (2015) to model the time-dependent chemical reactions in this study. We use the modified version of the GADGET-2 momentum equation from our previous study Dutta (2016a) to model external pressure boundary for both the idealized as well as realistic minihalos.

5.3 Angular Momentum

It is a common feature of all star formation calculations that the angular momentum of a single star or star-cluster is much lower than that of the original cloud in which the protostars form (e.g., Bodenheimer 1995). We follow the collapse of primordial gas and study the distribution of the angular momentum for different degrees of initial rotation (β_0).

Figure 5.1 shows the physical conditions in the gas once the central region has collapsed to a density of $\sim 5 \times 10^{13}$ cm^{-3}. The panels show mass-weighted averages of the properties of individual SPH particles within radial logarithmic bins. We find in Figure 5.1A that regardless of the initial rotation speed, all clouds closely follow a power-law density profile $n \propto r^{-2.2}$, implying to a relation between the radius and enclosed mass $M \propto r^{4/5}$ (Figure 5.1B). However, these are only approximate relations and different degrees of the rotational support in clouds leads to subtle deviations. For example, larger rotational support leads to a slightly steeper density gradient in the inner 10^4 AU, so that the enclosed mass within a certain radius is larger for the

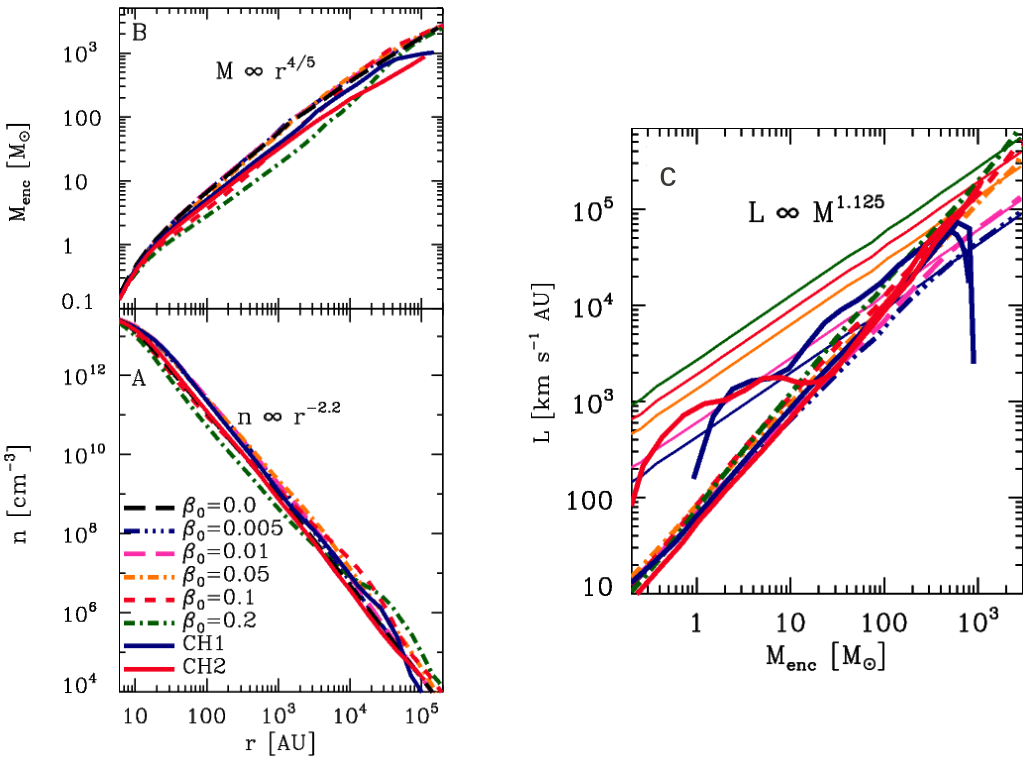

Figure 5.1: (A) Radial logarithmic binned, mass-weighted averages of the number density (n) and (B) enclosed gas mass within the radius (r) are plotted as a function of the radius for different degrees of initial rotation of the cloud (β_0), including for the non-rotating case ($\beta_0 = 0$). These plots are created just before the formation of the first protostar. The specific angular momentum follows a power-law relation with the enclosed gas mass irrespective of the cloud's initial configuration. The *solid lines* represent the initial state of the angular momentum (L_0) for the different β_0-modeled.

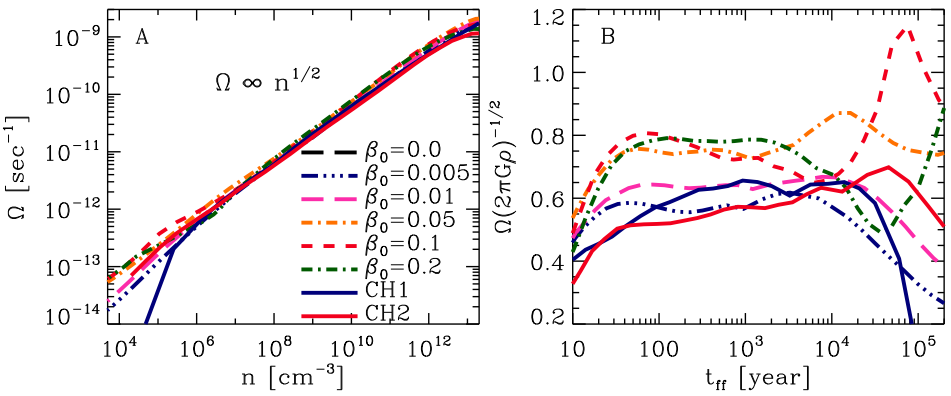

Figure 5.2: (A) Radially binned, mass-weighted averages of the angular velocity is plotted a function of the number density ($\Omega \propto n^{1/2}$) for different degrees of initial rotation (β_0). (B) Toomre's Q-parameter (defined as $Q = \Omega\sqrt{2\pi G\rho}$ (Matsumoto, Hanawa & Nakamura 1997) is nearly constant with the local free-fall time.

clouds with smaller β_0 values.

We plot the final and initial specific angular momentum profiles (i.e., angular momentum per unit mass shell) in Figure 5.1C as a function of the enclosed gas mass. The solid lines represent the cloud's initial specific angular momentum (L_0), while the dot-dashed lines describe the final state. We see that the specific angular momentum changes significantly, resulting in its redistribution during the gravitational contraction. For the final state, we find that $L \propto M^{1.125}$ irrespective of the initial rotation of the cloud. We also note in Figure 5.1A that it is the $\beta_0 = 0.2$ case that has the lowest values of n within the enclosed $10^3 M_\odot$ and the highest values of n outside this range at the evolutionary phase recorded here. That means cloud with $\beta_0 = 0.2$ has gone through an efficient phase of angular momentum distribution from the center to the periphery during the initial contraction.

This characteristic power-law behavior has been reported in several studies (e.g., Abel, Bryan & Norman 2002; Yoshida et al. 2006; Clark et al. 2011) using cosmological initial conditions that are very different from our idealized initial conditions. We find the scaling relations of the characteristic angular momentum profile in two completely different gas distribution: (1) in idealized minihalos of five different simulations (with β_0-model) and (2) in two realistic cosmological simulations. This experiment suggests

that the power-law angular momentum distribution is a natural outcome of the collapsing gas, and may be a fundamental and universal property of the gravitational collapse of the primordial star-forming cloud.

5.3.1 Origin of the power-law slope

Hydrodynamical calculations of the gravitational collapse (e.g., Omukai & Nishi 1998 have shown that all clouds converge towards a higher-density regime that roughly obeys the power-law relation $n \propto r^{-2.2}$. We find that the non-rotating clouds ($\beta_0 = 0$) also have the similar density profile like their rotating counterparts. Previous studies have shown that the collapse approaches a self-similar solution, well-known for the non-rotating case (Larson 1969). Even for rotating clouds, it appears that the collapse still proceeds in a self-similar fashion (Matsumoto, Hanawa & Nakamura 1997). From a dimensional analysis, one has $\Omega/\sqrt{G\rho} =$ constant, where Ω is the angular velocity of the rotating cloud. Hence we have $\Omega \propto n^{1/2} \propto R^{-1.1}$ (Figure 5.2A), followed by $\Omega \propto M^{-1.375}$. This leads to the angular momentum profile of the collapsed gas:

$$L \propto \Omega r^2 \propto M^{1.125}\,. \tag{5.1}$$

The relation in Figure 5.2A is also satisfied for a homogeneous cloud in centrifugal equilibrium. Even in that case, $\Omega_K = v_K/r = \sqrt{GM/r^3} \simeq \sqrt{G\rho(r)}$ for a mean density $\rho(r)$ within the radius r, where Ω_K is the angular velocity for Keplerian rotation. In Figure 5.2B, we show the Toomre Q-parameter defined as $Q = \Omega/\sqrt{2\pi G\rho}$ (Matsumoto, Hanawa & Nakamura 1997) plotted as a function of the free-fall time. As expected, the quantity $\Omega(2\pi G\rho)^{-1/2}$ is roughly constant with the free-fall time of the collapsed gas. We conclude that the angular velocity and the angular momentum follow a pivotal power-law relation with the enclosed mass and are independent of the initial rotation and turbulence of the cloud. At this point, we also note that the specific angular momentum for the final state of the collapse does not necessarily depend on the initial density configuration. As the collapse proceeds to protostellar densities, one can always obtain the power-law angular momentum profile for both the initial uniform density and centrally condensed distribution.

5.3.2 Discussion on angular momentum distribution

As the gas continues to collapse, the angular momentum is continually distributed to maintain the angular velocities that are significant fraction of the Keplerian velocities. Unlike the present-day star formation where the rotation rate is reduced by the magnetized stellar winds and magnetic braking (Matt et al. 2010), the process of transferring the angular momentum during the primordial collapse is ambiguous and of utmost interest. Since the initial strength of rotation of the clouds can significantly affect the thermal as well as dynamical evolution of gas, a higher angular momentum of clouds can have different properties than their slowly rotating counterparts (Hirano et al. 2014; Dutta 2016a).

We adopt a Lagrangian point of view to calculate the time derivative of the specific angular momentum ($\tau = dL/dt$) for different mass shells that are logarithmically binned mass-weighted averages of SPH particles. Following Yoshida et al. (2006), we can write the expression for two kinds of torques in the case of primordial gas collapse,

$$\begin{aligned} \frac{dL}{dt} &= \frac{d}{dt}\sum_{i=1}^{n}(\vec{r}_i \times \vec{v}_i) \\ &= \sum_{i=1}^{n}\vec{r}_i \times \left(\vec{F}_{\rm grav} + \vec{F}_{\rm pres}\right) \\ &= \vec{\tau}_{\rm grav} + \vec{\tau}_{\rm pres} \end{aligned} \tag{5.2}$$

where $\vec{F}_{\rm grav}$ is the total acceleration due to gravity, i.e., summation over all mass shell i, and $\vec{F}_{\rm pres}$ is the total force per unit mass due to the pressure gradients between the mass shells. We can therefore write the gravitational torques ($\tau_{\rm grav}$) and pressure torque ($\tau_{\rm pres}$) as following:

$$\vec{\tau}_{\rm grav} = \sum_{i=1}^{n}\vec{r}_i \times \frac{d\vec{v}_i}{dt} \tag{5.3}$$

$$\vec{\tau}_{\rm pres} = \sum_{i=1}^{n}\vec{r}_i \times \frac{\nabla\vec{P}_i}{\rho_i} \tag{5.4}$$

where $\vec{r}_i$ is the distance of the mass shell i from the center, $d\vec{v}_i/dt$ is the acceleration due to gravity of the ith shell, ρ_i is the density and ∇P_i is the pressure gradient between the shells. The sum goes over all SPH particles in spherical mass shell under consideration.

The gravitational torque is generated due to the nonaxisymmetric nature of the collapsing cloud or due to the spiral structure (e.g., Yoshida, Omukai & Hernquist 2008; Lin, Krumholz & Kratter 2011). For a rotating collapsing core, the non-radial gravitational forces due to the irregularities in the structure can produce a trailing spiral feature of large amplitude (Larson 1984). The associated gravitational torques can then transfer angular momentum outward on an orbital time-scale. In the case of a clustered formation, the angular momentum could be efficiently transported outward by tidal torques, similar to the case of present-day star formation in a clustered environment (Bate, Bonnell & Bromm 2003). Gravitational torques associated with gravitational instabilities also become important for angular momentum transport and energy dissipation in a self-gravitating accretion disk within a local viscous framework (Lodato & Rice 2004). However, for a rotating collapsing core we find that the density gradient between the shells can produce the non-radial pressure torque. The concept of transferring angular momentum due to the pressure torque may be equivalent with the transport of angular momentum via hydrodynamic shocks during the turbulent collapse (as discussed in Abel, Bryan & Norman 2002).

For all β_0 modeled, we take into account both kinds of forces in our simulations: one is the acceleration due to gravity that leads to the gravitational torque ($\tau_{\rm grav}$) and another is the pressure-torque ($\tau_{\rm pres}$). Here we refer the study by Larson (1984), which concluded that the non-axisymmetric nature of the cloud or inhomogeneities tend to form a spiral structure that produces the gravitational torque. The pressure forces can arise from the density gradient between the mass shells. We have observed that the gravitational and pressure torques act in opposite directions, though not always, and change direction throughout the collapsing gas cloud. However, the contribution of the torques will be more clear in terms of change of angular momentum that is shown in Figure 5.3.

Taking the fractional change in the angular momentum of a shell ($\Delta L(r)/L(r)$)

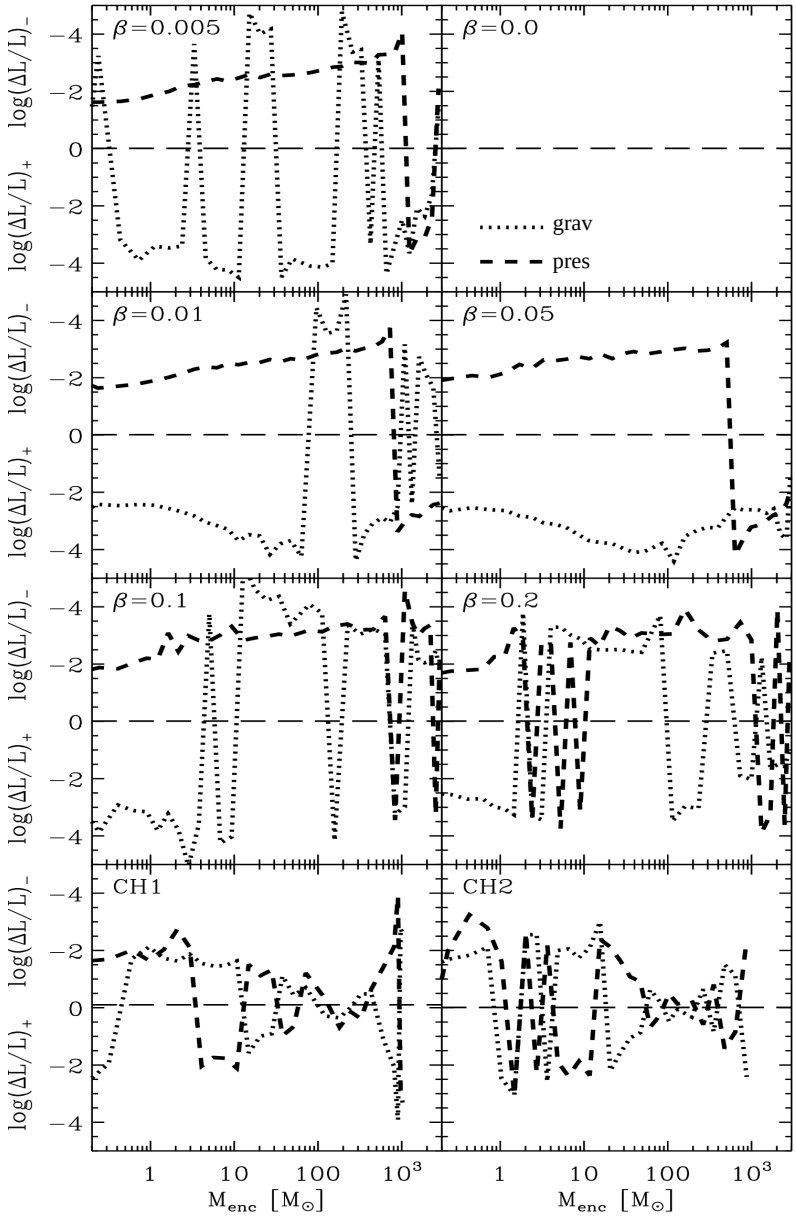

Figure 5.3: The fractional change of the specific angular momentum ($\Delta L/L$) with the free-fall time of the mass shell due to the torques acting on the shell are plotted as a function of enclosed gas mass, just before formation of first protostar. The sign implies whether the angular momentum is gained (positive) or lost (negative) during collapse.

with the local free-fall time ($t_{\rm ff}$), we find that both the torques are dominant throughout the evolution. As the collapse proceeds to higher densities, the angular momentum of a shell can increase or decrease depending on whether torques acting on the shell are positive or negative. We use $(\Delta L/L)_+$ and $(\Delta L/L)_-$ for the positive and negative fractional change of each type of torque (Figure 5.3). The net change in the angular momentum happens due to the synchronous action of both the gravitational and pressure torques. However, in the inner regime, the cloud gains angular momentum due to the pressure gradient between the mass shells. On the other hand cloud's angular momentum is lost due to torque exerted by the gravity. This is consistent with the recent work by Greif et al. (2012) that concluded that the gravitational torque tends to decreases the angular momentum whereas the pressure torque does the opposite during the collapse of gas towards the protostellar densities. The spiral structure of the Keplerian disk that becomes gravitationally unstable can transfer the mass inside, thereby removing the extra angular momentum in the outward direction (Becerra et al. 2015). In addition, cosmological hydrodynamics simulations by Wise, Turk & Abel (2008) have shown that the rotational secular bar instabilities can efficiently transport angular momentum outward in the central regime. It has also been suggested that for a simple hydrodynamical flow, the Reynolds stress associated with velocity fluctuations might act as a turbulent transport, and angular momentum can then be removed from the mean flow (Lodato 2008).

5.4 Summary and discussion

We have investigated in detail the angular momentum evolution during the collapse of the primordial gas and analyzed its relation with other physical quantities. For this purpose, we have followed a systematic parameter study that spans two orders of magnitude in the strength of rotational support for the idealized solid body rotation along with two realistic cosmological minihalos.

We find that the initial configuration of the gas clouds (e.g., rotation, turbulence and halo-to-halo variation) have little influence on the distribution of the cloud's specific angular momentum. Apart from the well-known density distribution, we find that

the angular momentum also provides another way of explaining the properties of the primordial gas collapse. In addition, the sole dependency of the angular momentum on the gas mass makes it easier to understand the primordial star formation. These basic characteristics of the angular momentum distribution make it to be the fundamental property of the primordial gas collapse. We also discuss the possible mechanisms that are responsible for the power-law profile of angular momentum, mainly the simultaneous effect of the gravitational and pressure torques. We argue that the distribution is due to internal torques only and does not require the presence of turbulence or magnetic fields. However, the exact way of transferring the angular momentum, and whether or not it is related to the other physical properties, need further theoretical investigation.

The angular momentum distribution is an area of active research. There have been various investigations in a number of previous studies for the transport issues. For example, from the forefront studies by Larson (1969) to present theoretical studies (e.g., Yoshida et al. 2006; Bromm 2013; Hirano et al. 2015), people have tried to describe the plausible causes of the angular momentum transport especially for a system where magnetic fields have less or no contribution. The gravitational collapse of primordial gas is considered to be weakly magnetized (although recent simulations are showing the influence of the magnetic field, e.g., Sur et al. 2010). In such system, the pressure and gravitational torques could play an important role (although some studies consider only gravitational torque). We have performed a set of high-resolution simulations with varied rotation parameter (β_0) to study the angular momentum distribution. For the first time, to the best our knowledge, we have shown the effect of both the pressure torque as well as gravitational torque. Although our approach is different, we obtain similar results from previous investigations (e.g., Yoshida et al. 2006; Greif et al. 2012). Our primary aim in this study was to investigate the distribution of the angular momentum, and we have shown how the distribution is related to the physical parameter of the collapsing gas. However, in describing the distribution along with the scaling relation, we have also made an attempt to discuss how the power-law behavior is controlled during the collapse. From our investigation, we can conclude that the distribution of angular momentum happens due to the concurrent

effects of internal torques in a collapsing system where turbulence or magnetic field does not play any significant role.

At this point, we would like to emphasize that we have discussed the possible source of transport only for a weakly magnetised Pop III collapse (Tan & McKee 2004; Bromm, Yoshida, Hernquist & McKee 2009). On the other hand, the study by DeSouza & Opher (2008) has shown that the magnetic field plays an important role during collapse. The most common explanation for transfer of angular momentum is magnetized stellar winds and magnetic outflow (see e.g. Matt & Pudritz 2005). It has also been suggested that accretion disks threaded by a weak magnetic field are subject to magneto-hydrodynamics (MHD) instabilities (Balbus & Hawley 1998), which can induce turbulence in the disk, thereby being able to transport angular momentum and to promote the accretion process. However, in many astrophysical phenomena, such as the outer regions of protostellar disks, the ionization level is expected to be low, significantly reducing the effects of magnetic fields in determining the dynamics of the disk (Gammie 1996).

More recently the numerical simulations show the amplification of small seed fields up to dynamically important strengths during the collapse of primordial star-forming halos (Sur et al. 2010, 2012; Schleicher et al. 2010; Schober et al. 2012). The angular momentum can then be transported in the protostellar disk via magnetic braking (Machida & Doi 2013). However, the influence of the amplified magnetic fields on the redistribution of angular momentum requires further investigation.

Chapter 6

Conclusions and Future Work

We have investigated in detail the collapse of primordial star-forming clouds and the resulting fragmentation of the circumstellar accretion disk. For this purpose, we performed a set of three-dimensional hydrodynamical simulations using GADGET-2 SPH code to follow the gas collapse beyond the point at which the first protostar forms. We follow the chemical, thermal and dynamical evolution of the gas in both idealized as well as more realistic minihalos in order to assess the differences introduced by varying halo parameters. We have also followed a systematic parameter study that spans two orders of magnitude in the strength of rotational support for the solid body rotation to study the angular momentum distribution during collapse. The main findings of this dissertation can be summarized as follows.

- We find that the uncertainty in the three-body H_2 formation rates leads to the differences in the chemical state of the gas which is more important for the thermal evolution of the clouds than any differences in the halo properties. The halo-to-halo variation affects the dynamical evolution of the gas and mass-accretion more than the chemical uncertainties. This difference is roughly a factor of 2, however, is comparable to the halo-to-halo variation.

- The thermal instability need not necessarily be the criterion for possible fragmentation. Instead, fragmentation occurs when H_2 cooling, the heat released by H_2 formation, and compressional heating together set the Jeans mass in the

gas to values that are conducive to breakup and collapse. This leads the disk to fragment on a scale of 1000–2000 AU.

- The cloud's initial degree of rotation initiates a significant impact on the heating and cooling process, which leads to a scatter in the temperature evolution of the collapsing gas. A higher degree of rotation can hinder the infall, lead to a cooler gas, and result in more fragmentation. In addition, we find that the protostars with higher rotational support have larger spiral arms with lower accretion rates. We also point out that the newborn protostars are distributed in such a way to conserve the angular momentum, and some of them could have survived until today if they were of sufficiently low mass.

- The power-law angular momentum distribution is a natural outcome of the collapsing gas, which is controlled by the simultaneous effect of the gravitational and pressure torques, and does not depend on the initial degree of rotation and turbulence of the gas clump. In addition, the sole dependency of the angular momentum on the gas mass makes it easier to understand the primordial star formation. These basic characteristics of the angular momentum distribution make it to be the fundamental property of the primordial gas collapse.

- We conclude that fragmentation of the circumstellar disk highly depends on the initial configuration of the unstable gas clump. Therefore, the use of appropriate initial conditions of the gas in minihalos is a pivotal and decisive quantity to study the gas evolution during collapse and final fate of the Pop III stars.

6.1 Future Plan

There are various research projects that can be done by adding more physics with the current simulation set-up. The next step is to study the detailed modeling of the primordial magnetic field and radiative feedback in a set of calculations. This will include the heating and modified chemistry driven by Pop III emission of H_2-dissociating Lyman-Werner radiation and ionizing radiation. These simulations will

allow us to directly investigate the growth of the radiation field emanating from Pop III stars and their influence in the evolution of the surrounding regions. This would be larger than simulations done for my thesis work, and would therefore be more physically realistic to address many important issues such as the formation and evolution of first galaxies and Super-Massive Black Holes (SMBHs).

Understanding the first stars and galaxies is of utmost interest. They released copious amount of ultraviolet light to carve out ionized medium around them. To what extent did the radiative feedback and magnetic field synchronize their formation and evolution? In addition, the semi-numerical simulation along with the detection of the 21cm signal can provide an important insight into the early universe, for example, how galaxies such as our own Milky Way formed. The cosmological 21cm signal is sensitive to both the ionization and the thermal history of the cosmic gas.

An improved knowledge of the SMBHs can provide the physical condition within the first 800 Myr after the Big Bang. Simultaneously, we can study the evolution of galaxies that host the SMBHs and their role on the gas dynamics, ionization structure and star forming activity. Measuring the most distance galaxies is crucial in comprehending the universe when it was extremely young. The recent observations along with state-of-the-art instruments and surveys such as GMRT, ALMA, JWST promise to provide a powerful probe for our current understanding.

In summary, there are number of works that can be done on the dynamics of the primordial gas collapse to understand the early universe. These works will endeavour the ultimate goal of understanding the high-redshift universe. I am excited to become part of such scientific projects and looking forward to continue study of this topic in the years to come.

Bibliography

Abel, T., Anninos P., Norman, M. L., Zhang Y., 1998, ApJ, 508, 518

Abel, T., Bryan, G. L. & Norman, M. L. 2000, ApJ, 540, 39

Abel, T., Bryan, G. L. & Norman, M. L. 2002, Science, 295, 93

Abel, T., Wise, J. H., Bryan, G. L., 2007, ApJ, 659L, 87A

Balbus, S. A., Hawley, J. F. 1998, Rev. Mod. Phys. 70, 1

Bodenheimer, P. 1995, ARA&A, 33, 199B

Barkana, R., Loeb, A., 2001, Phys. Rep., 349, 125

Bate, M. R., Bonnell, I. A. & Price, N. M. 1995, MNRAS, 277, 362

Bate, M. R., Burkert, A., 1997, MNRAS, 288, 1060 B

Bate M. R., Bonnell I. A., Bromm V. 2003. MNRAS 339, 577

Becerra, F., Greif, T. H., Springel, V., Hernquist, L. E, 2015, MNRAS, 446, 2380B

Bovino, S., Schleicher, D. R. G., Grassi, T., 2014, A&A, 561A, 13B

Bromm, V., Coppi, P. S., & Larson, R. B., 1999, ApJ, 527L, 5B

Bromm, V., Coppi, P. S., & Larson, R. B. 2002, ApJ, 564, 23

Bromm, V., & Larson, R. B. 2004, ARA&A, 42, 79

Bromm, V., Yoshida, N., Hernquist, L. & McKee, C. F. 2009, Nature, 459, 49

Bromm, V., Yoshida, N., 2011, ARA&A 49, 373

Bromm, V., 2013, RPPh, 76k2901B

Bonnor, W., B. 1956, MNRAS, 116, 351

Ciardi, B. & Ferrara A, 2005, Space Sci. Rev., 116, 625

Chabrier, G., 2003, PASP, 115, 763

Clark, P. C., Glover, S. C. O., & Klessen, R. S. 2008,ApJ, 672, 757

Clark, P. C., Glover, S. C. O., Klessen, R. S. & Bromm, V. 2011a, ApJ 727 110

Clark, P. C., Glover, S. C. O., Smith, R. J., Greif, T. H., Klessen, R. S. & Bromm, V. 2011b, Science, 331, 1040

Couchman, H. M. P., Rees, M. J., 1986, MNRAS, 221, 53C

de Souza, R. S.& Opher, R., 2008, PhRvD, 77d, 3529D

de Avillez, Miguel A., Asgekar, A., Breitschwerdt, D., Spitoni, E., 2012, MNRAS, 423L, 107D

Dicke, R. H., Peebles, P. J. E., Roll, P. G., Wilkinson, D. T., 1965, ApJ, 142, 414D

Dopcke, G., Glover, S C. O., Clark, P. C., Klessen, R. S., 2013, ApJ, 766, 103D

Dutta, J, Clark, P. C., Klessen, R. S., AIP Conference Proceedings, Vol 1480, pp. 333-336, 2012 (Best Poster Prize)

Dutta, J, Nath, B, B., Clark, P. C., Klessen, R. S., 2015, MNRAS, 450, 202D

Dutta, J., 2015a, ApJ, 811, 98D

Dutta, J., A&A, 585A, 59D, 2016

Dutta, J., Ap&SS, 361, 35D, 2016

Ebert, R., Z. 1955, Astrophys, 37, 217

Fisher R. T. 2004, Astrophys. J. 600 76980

Federrath, C.; Banerjee, R.; Clark, P. C.; Klessen, R. S., 2010, ApJ, 713, 269F

Federrath, C., Sur S., Schleicher D. R. G., Banerjee R. & Klessen R. S., 2011, ApJ, 731, 62

Flower, D. R., & Harris, G. J. 2007, MNRAS, 377, 705

Furlanetto, S., Mesinger, A., 2009, MNRAS, 394, 1667F

Forrey, R. C., 2013, ApJ, 773L, 25F

Frebel, A., Aoki, W., Christlieb, N., Ando, H., Asplund, M., Barklem, P. S., Beers, T. C., Eriksson, K., Fechner, C., Fujimoto, M. Y., Honda, S., Kajino, T., Minezaki, T., Nomoto, K., Norris, J. E., Ryan, S. G., Takada-Hidai, M., Tsangarides, S., Yoshii, Y., 2005, Natur, 434, 871F

Gammie, C. F., 1996, ApJ, 457, 355

Glover, S. 2005, Space Sci. Rev., 117, 445

Glover, S. C. O. 2008, in First Stars III, Chemistry and Cooling in Metal-Free and Metal-Poor Gas, eds. B. O'Shea, A. Heger, (New York: AIP), 25, 990, 25G

Glover, S. C. O., & Abel, T. 2008, MNRAS, 388, 1627

Glover, S. C. O. & Savin, D. W., 2009, MNRAS, 393, 911

Glover, S., 2013, ASSL, 396, 103G

Greif, T. H., Springel, V., White, S. D. M., Glover, S. C. O., Clark, P. C., Smith, R. J., Klessen, R. S., Bromm, V., 2011, ApJ, 737, 75G

Greif, T. H., Bromm, V, Clark, P. C., Glover, S. C. O., Smith, R. J., Klessen, R. S., Yoshida, N., Springel, V, 2012, MNRAS, 424, 399G

Greif, T. H., Springel, V., Bromm, V, 2013, MNRAS, 434, 3408G

Greif, T. H., 2014, MNRAS, 444, 1566G

Greif, T. H., 2015, ComAC, 2, 3G

Haiman, Z., Thoul, A. A., Loeb, A, 1996, ApJ, 464, 523H

Heger, A. & Woosley, S. E., 2002, ApJ, 567, 532H

Hirano, S., Yoshida, N., 2013, ApJ, 763, 52H

Hirano, S., Hosokawa, T., Yoshida, N., Umeda, H., Omukai, K., Chiaki, G., Yorke, H., 2014, ApJ, 781, 60H

Hirano, S., Hosokawa, T., Yoshida, N., Omukai, K., Yorke, H., 2015, MNRAS, 448, 568H

Hartwig, T., Clark, P. C., Glover, S. C. O., Klessen, R. S., Sasaki, M., 2015, ApJ, 799, 114H

Hosokawa, T., Omukai, K., Yoshida Naoki & Yorke H. W. 2011, Science, 334, 1250

Jappsen, A.-K.; Klessen, R. S., 2004, A&A, 423, 1J

Jappsen, A. K., Klessen, R. S., Larson, R. B., Li, Y. & Mac Low, M. M. 2005, A&A, 435, 611

Johnson, J. L., Greif T. H., Bromm, V., 2007, ApJ, 665, 85J

Johnson, J. L., Dalla V. C., Khochfar, S., 2013, MNRAS, 428, 1857J

Johnson, J. L., Dalla V. C., Khochfar, S., 2013, MNRAS, 428, 1857J

Klessen, R. S., Glover, S. C. O., lecture notes of the 43rd Saas Fee Advanced Course *Star Formation in Galaxy Evolution: Connecting Numerical Models to Reality*, ed. Y. Revaz (Springer Publishing), arXiv:1412.5182

Kroupa, P., 2002, Science, 295, 82

Kitayama, T., Yoshida, N., Susa, H., Umemura, M., 2004, ApJ, 613, 631K

Krumholz, M. R., McKee, C. F. & Klein, R. I., 2004, ApJ, 611, 399

Latif, M. A., Schleicher, D. R. G., Schmidt, W., Niemeyer, J., 2013, ApJ, 772L, 3L

Latif, M. A. & Schleicher, D. R. G., 2015, A&A, 578A, 118L

Latif, M. A. & Schleicher, D. R. G., 2015, MNRAS, 449, 77L

Lin Min-Kai, Krumholz M. R., Kratter K. M., 2011, MNRAS, 416, 580L

Larson, R. B., 1969, MNRAS, 145, 271L

Larson, R. B., 1972, MNRAS, 156, 437L

Larson, R. B. 1984, MNRAS, 206, 197

Lodato G., Rice W. K. M., 2004, MNRAS, 351, 630L

Lodato G., 2008, NewAR, 52, 21L

Loeb, A., & Wyithe, J. S. B., 2008, PhRvL, 100, p1301L

Loeb A., 2010, How Did the First Stars and Galaxies Form? Princeton Univ. Press, Princeton

Lopes, I., Casanellas, J.,Eugnio, D., 2011, PhRvD, 83f3521L

Lopes, I. & Silk, J., 2014, ApJ, 786, 25L

McDowell, M. R. C., 1961, observatory, 81, 240

Matsumoto, T., Hanawa, T., Nakamura, F., 1997, ApJ, 478, 569

Mather et al, 1990, ApJ, 354L, 37M, Preliminary results from the COBE

Madao, P., 2000, PhST, 85, 156M, Proceedings of Nobel Symposium 109

Madau, P., Ferrara, A., Rees, M. J., 2001, ApJ, 555, 92M

McKee C. F. & Tan, J. C., 2008, ApJ, 681, 771

Mac Low M.-M., Ferrara A., 1999, ApJ, 513, 142

Mesinger, A., Johnson, B. D., Haiman, Z., 2006, ApJ, 637, 80M

Meynet, G., 2009, LNP, 765, 139M

Machida, M. N., Matsumoto, T. & Inutsuka, S., 2008, ApJ, 685

Machida, M. N., Omukai, K., Matsumoto, T. & Inutsuka, S. i., 2008, ApJ, 677, 813

Machida, M. & Doi, K., 2013, MNRAS, 435, 3283M

Matt, S., Pudritz, R. E. 2005 MNRAS, 356, 167

Matt, S. P., Pinzn G., de la Reza R., Greene, T. P., 2010, ApJ, 714, 989

Miralda-Escudé, J., 2003, Science, 300, 1904M

Maiolino, R., Schneider, R., Oliva, E., Bianchi, S., Ferrara, A., Mannucci, F., Pedani, M., Roca Sogorb, M., 2004, Nature, 431, 533M

Norman, M. L., Wilson, J. R., Barton, R. T., 1980, ApJ, 239, 968N

Norman, M. L., O'Shea, B. W., Paschos, P., 2004, ApJ, 601L, 115N

Oh S. P., Haiman Z., 2002, ApJ, 569, 558

Omukai, K. & Nishi, R. 1998, ApJ, 508, 141

Omukai, K., 2000, ApJ, 534, 809-824

Omukai K., Yoshii Y., 2003, ApJ, 599, 746

Omukai, K., Tsuribe, T., Schneider, R., & Ferrara, A. 2005, ApJ, 626, 627

Orel, A. E., 1987, J. Chem. Phys., 87, 314

O'Shea, B. W. & Norman, M. L. 2006, ApJ, 648, 31

O'Shea, B. W., & Norman, M. L. 2007, ApJ, 654, 66

O'Shea, B. W. & Norman, M. L., 2008, ApJ, 673, 14O

Palla, F., Salpeter, E. E. & Stahler, S. W. 1983, ApJ, 271, 632

Planck Collaboration Ade P. A. R., Aghanim N., Armitage Caplan C., Arnaud M., Ashdown M., Atrio-Barandela F., Aumont J., Baccigalupi C., Banday A. J., et al. 2014, A&A, 571, A16

Peebles, P. J. E., Dicke, R. H, 1968, ApJ, 154, 891P

Penzias, A. A., Wilson, R. W., 1965, ApJ, 142, 1149P

Perlmutter, S. et al., 1999, ApJ, 517, 565P

Reed, D. S.; Bower, R.; Frenk, C. S.; Gao, L.; Jenkins, A.; Theuns, T.; White, Simon D. M., 2005, MNRAS, 363, 393R

Riess, Adam G. et al., 1998, AJ, 116, 1009R

Ripamonti, E. & Abel, T. 2004, MNRAS, 348, 1019

Ritter, J. S., Safranek-Shrader, C., Gnat, O., Milosavljevi, M., Bromm, V., 2012, ApJ, 761, 56R

Sabano Y. & Yoshii Y., 1977, PASJ, 29, 207

Saslaw, W. C. & Zipoy, D., 1967, Natur, 216, 976S

Silk, J., 1977, ApJ, 211, 638S

Silk J., 1983, MNRAS, 205, 705

Schneider, R.; Ferrara, A.; Salvaterra, R.; Omukai, K.; Bromm, V., 2003, Nature, 422, 869S

Schneider, R., Salvaterra, R., Ferrara, A., Ciardi, B., 2006, MNRAS, 369, 825S

Schaye, J., Aguirre, A., Kim, Tae-Sun., Theuns, T., Rauch, M., Sargent, W. L. W., 2003, ApJ, 596, 768S

Schober J., Schleicher D. R. G., Federrath C., Glover, S., Klessen R. S., Banerjee R. 2012, ApJ, 754, 99S

Sur, S., Schleicher D. R. G., Banerjee R., Federrath C. & Klessen R. S. 2010, ApJ, 721, L134

Sur, S., Federrath C., Schleicher D. R. G., Banerjee R., & Klessen R. S. 2012, MNRAS, 423, 3148S

Schleicher, D. R. G., Banerjee, R., Sur, S., Arshakian, T. G., Klessen, R. S., Beck, R. & Spaans, M., 2010, A&A, 522, A115

Saigo, K., Tomisaka, K., Matsumoto, T., 2008, ApJ, 674, 997S

Scannapieco, E., Schneider, R., Ferrara, A., 2003, ApJ, 589, 35S

Smith, R. J., Glover, S. C. O., Clark, P. C., Greif, T., Klessen, R. S., 2011, MNRAS, 414, 3633S

Sobral, D., Matthee, J., Darvish, B., Schaerer, D., Mobasher, B., Rttgering, H. J. A., Santos, S., Hemmati, S., 2015, ApJ, 808, 139S

Smoot et al, 1991, ApJ, 371L, 1S, Preliminary results from the COBE

Susa, H., Uehara, H., Nishi, R., Yamada, M., 1998, PThPh, 100,63S

Susa, H., 2013, ApJ, 773, 185S

Springel, V., White, S. D. M., Jenkins, A., Frenk, C. S., Yoshida, N., Gao, L., Navarro, J., Thacker, R., Croton, D., Helly, J., Peacock, J. A., Cole, S., Thomas, P., Couchman, H., Evrard, A., Colberg, J., Pearce, F., 2005, Nature, 435, 629S

Springel, V., 2005, MNRAS, 364, 1105

Springel, V., 2010, MNRAS, 401, 791S

Sterzik, M. F., Durisen, H. & Zinnecker, H., 2003, A&A, 411, 91S

Stacy, A., Greif, T. H. & Bromm, V. 2010, MNRAS, 403, 45

Stacy, A., Bromm, V, & Loeb, A., 2011, MNRAS 413, 543

Stacy, A., Greif, T. H. & Bromm, V., 2012, MNRAS, 422, 290S

Stacy, A., Greif, T. H., Klessen, R. S., Bromm, V. & Loeb, A, 2013, MNRAS, 431, 1470S

Stacy, A. & Bromm, V., 2013, MNRAS, 433, 1094S

Tan, J. C., & McKee C. F., 2004, ApJ, 603, 383

Tegmark, M., Silk, J., Rees, M. J., Blanchard, A., Abel, T., Palla, F., 1997, ApJ, 474, 1T

Tornatore, L., Ferrara, A., Schneider, R., 2007, MNRAS, 382, 945T

Tornatore, L., Borgani, S., Dolag, K., Matteucci, F., 2007, MNRAS, 382, 1050T

Tumlinson, J. & Shull, J. M., 2000, ApJ, 528L, 65T

Turk, M. J., Abel, T. & O'Shea, B. W. 2009, Science, 325, 601

Turk, M. J., Clark, P. C., Glover, S. C. O., Greif, T. H., Abel, T., Klessen, R. S. & Bromm, V., 2011, ApJ, 726

Umeda, H. & Nomoto, K., 2003, Natur, 422, 871U

Vasiliev, E. O., Vorobyov, E. I., Shchekinov, Yu. A., 2010, ARep, 54, 890V

Venkatesan, A., Schneider, R., Ferrara, A., 2004, MNRAS, 349L, 43V

Wada, K., Venkatesan, A., 2003, ApJ, 591, 38W

Wise, J. H. & Abel, T., 2007, ApJ, 665, 899

Wise, J. H., Turk, M. J., Abel, T., 2008, ApJ, 682, 745W

Wise, J. H. & Abel, T. 2008, ApJ, 685, 40

Whalen, D., O'Shea, B. W., Smidt, J., Norman, M. L., 2008, ApJ, 679, 925W

Whalen, D., Hueckstaedt, M., McConkie, O., 2010, ApJ, 712, 101W

Yoshida, N., Abel, T., Hernquist, L. & Sugiyama, N., 2003, ApJ, 592, 645Y

Yoshida, N., Omukai, K., Hernquist, L. & Abel, T. 2006, ApJ, 652

Yoshida, N., Omukai, K. & Hernquist, L. 2007, ApJ, 667, L117

Yoshida, N., Omukai, K. & Hernquist, L. 2008, Science, 321, 669

UNIVERSIDADE DE ÉVORA
INSTITUTO DE INVESTIGAÇÃO
E FORMAÇÃO AVANÇADA

Contactos:
Universidade de Évora
Instituto de Investigação e Formação Avançada — IIFA
Palácio do Vimioso | Largo Marquês de Marialva, Apart. 94
7002 - 554 Évora | Portugal
Tel: (+351) 266 706 581
Fax: (+351) 266 744 677
email: iifa@uevora.pt